Title: Reconstructing the retreat dynamics of the Bjørnøyrenna Ice Stream based on new 3D seismic geomorphology from the central Barents Sea.

Emilia D. Piasecka[1], Monica C.M. Winsborrow[2], Karin Andreassen[2], Chris R. Stokes[3]
(1) Department of Geology/CAGE, Centre for Arctic Gas Hydrates, Environment and Climate UiT The Arctic University of Norway
(2) CAGE, Centre for Arctic Gas Hydrates, Environment and Climate, UiT The Arctic University of Norway
(3) Department of Geography, Durham University, UK

Abstract: The stability of contemporary ice sheets is influenced by the discharge from ice streams - corridors of fast-flowing ice bounded by ice flowing an order of magnitude slower. Reconstructions of palaeo-ice stream dynamics contributes to our understanding of ice stream sensitivity to the ocean-climate system and can aid in the numerical modelling and prediction of future changes in contemporary ice sheets. Here we use 3D seismic data, covering 13,000 km^2 in the central Bjørnøyrenna (Bear Island Trough), Barents Sea, to investigate the record of ice streaming preserved on the seafloor and on a buried palaeoseafloor surface. The unusually broad coverage and high resolution of the dataset, as well as its location in the central area of the trough, enables improved reconstruction of dynamics of the former Bjørnøyrenna Ice Stream in terms of number of streaming events, their trajectory, and their relative age sequence during deglaciation. Our results reveal major changes in the configuration and flow dynamics of the ice stream, with up to 10 flow-switching events identified. For the first time, we also document ice streaming sourced from the eastern Barents Sea around the time of the LGM. This high degree of flow variability is suggested to have resulted from climate-driven changes in ice sheet geometry (and ice divide migration), and variations in topography that influenced calving at the ice stream terminus.

1. Introduction

The nature and distribution of glacial sediments and landforms provide insight into the spatial extent, thickness, and dynamics of former ice sheets. Studying the nature of palaeo-ice sheets and the factors which contribute to their demise is important with regard to understanding the dynamics of contemporary ice sheets and predicting their response to future climate change (Golledge et al., 2015; Pollard and DeConto, 2009; Ritz et al., 2015; Stokes et al., 2015). The stability of both former and contemporary marine-based ice sheets is primarily controlled by the discharge of the ice-mass through ice streams, and understanding their behaviour is of critical importance (Jamieson et al., 2012; King et al., 2009; Spagnolo et al., 2016; Stokes et al., 2016). Reconstructing palaeo-ice stream behaviour and their influence on deglaciation provides a long-term perspective of such processes and, as such, can provide insight into dynamic changes that might be expected in contemporary ice sheets and how they might impact on sea level.

The former Barents Sea Ice Sheet (BSIS) was a marine-based ice sheet, occupying the Barents Sea during the Late Weichselian (Fig. 1) and has been viewed as an analogue for the marine-based West Antarctic Ice Sheet (WAIS) (Jakobsson et al., 2014). Furthermore, the Bjørnøyrenna Palaeo-Ice Stream – the largest palaeo-ice stream in the Eurasian Arctic – has been likened to extant West Antarctic Ice Streams (Siegert and Dowdeswell, 2002). As such, detailed information about the dynamics of the Bjørnøyrenna Palaeo-Ice Stream, and how it influenced wider ice sheet stability, can provide important insights into the magnitude and rate of ice sheet deglaciation, with potential implications for the behaviour of the WAIS. In this study, a large high-resolution, industry 3D seismic dataset has been used to map a complex assemblage of over 3500 glacial landforms on the seafloor and a buried palaeo-seafloor surface (Upper Regional Unconformity: URU) of the former bed of the Bjørnøyrenna Ice Stream, SW Barents Sea. The unusually broad coverage of the study (~13000 km^2), compared to previous

work, permits investigation of the landform pattern on a large scale. These results are used to reconstruct past ice flow directions, ice flow extent and dynamics of the previously little-studied central Bjørnøyrenna.

The key questions motivating this study are:

- How many streaming events were there and how did the streaming direction change during deglaciation?
- Where were the major ice domes and divides located and how did they migrate through deglaciation?
- What are the controls behind the Bjørnøyrenna Ice Stream flow-switching?

2. Study area

2.1. Geology and topography

The Barents Sea is a relatively shallow epicontinental basin, extending over one of the widest continental shelves in the world (Fig. 1, inset). It is bordered by the Svalbard Archipelago to the NW, Novaya Zemlya to the NE, and the Norwegian and Russian coast to the S. The topography of the Barents Sea is characterised by shallow banks (water depths << 200 m) and several overdeepened cross-shelf troughs (water depths > 500 m). The most prominent topographic trough in the Barents Sea is Bjørnøyrenna (Fig.1A), which is ~1000 km long, 100-200 km wide, and extends from the E coast of Svalbard, opening towards the Norwegian Sea at the W shelf break.

Sediment cover in the Barents Sea is thin (generally less than 100 m), although in some areas (e.g. offshore Norway) it reaches 200-300 m (Solheim and Kristoffersen, 1984). Across large parts of the Barents Sea, the Upper Regional Unconformity (URU), an erosional boundary, separates pre-Tertiary sedimentary rocks from the overlying layers of glacigenic sediments (Faleide et al., 1996; Solheim et al., 1996). URU is an erosional geological boundary that, in the study area, lies at depths of approximately 57-63 m below the contemporary seabed (assuming a velocity of 1800 m/s for glacial sediments (Sættem et al., 1992)). Bjørnøyrenna is bounded on both sides by shallow flanks (<200 m), associated with structural geological boundaries (Fig.1B). This difference in inclination between the deep trough and the flanks is of tectonic origin, and driven by subsidence. Large fault complexes crosscut Bjørnøyrenna along its axis: the Bjørnøyrenna Fault Complex in the south and Hoop Fault Complex in the central part (Sigmond, 1992).

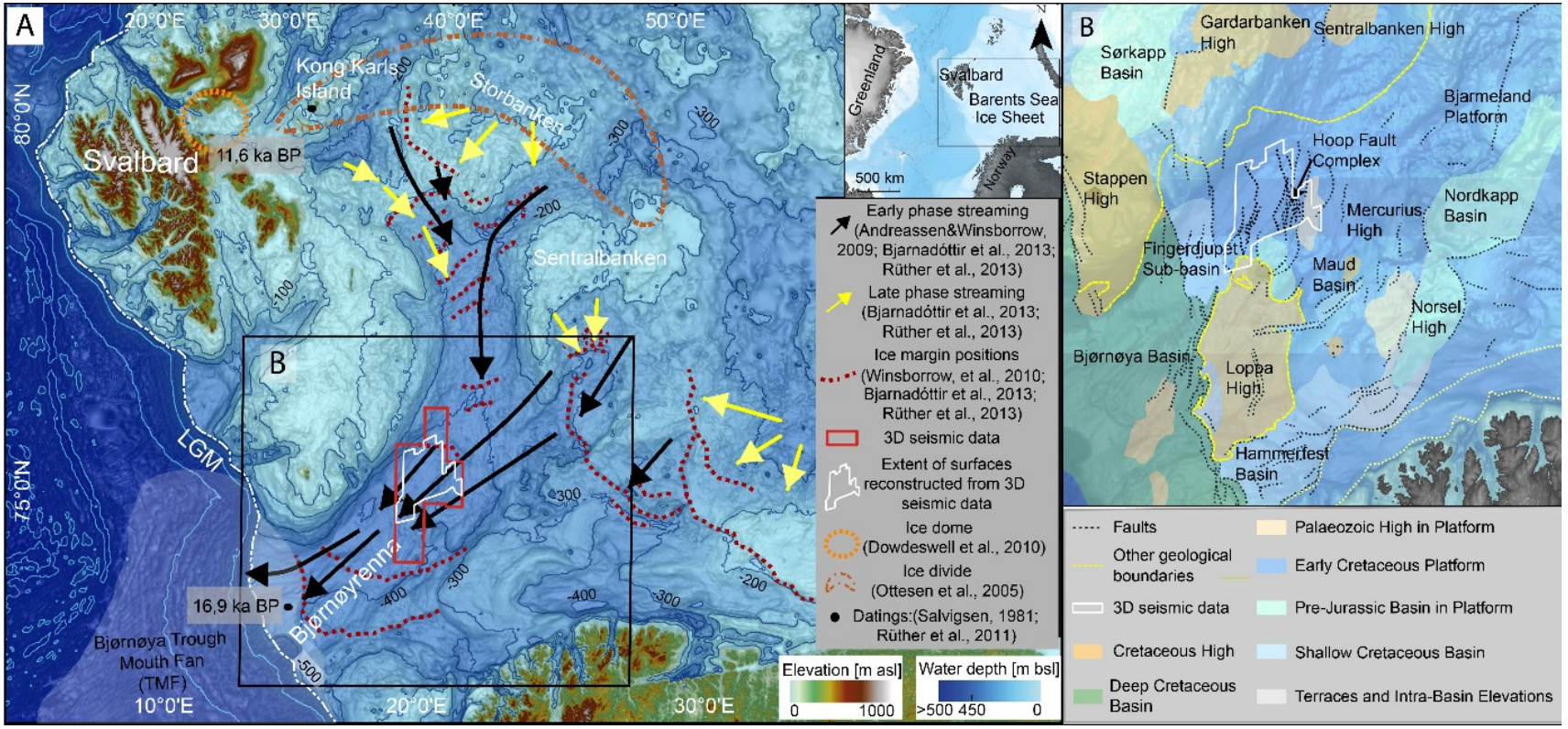
A
20°0'E
30°0'E
40°0'E
50°0'E
80°0'N
75°0'N
10°0'E
20°0'E
30°0'E
Kong Karls Land
Svalbard
11,6 ka BP
16,9 ka BP
Storbanken
Sentralbanken
Bjørnøyrenna
LGM
Bjørnøya Trough Mouth Fan (TMF)
B
-100
-200
-300
-400
-500
Greenland
Svalbard
Barents Sea Ice Sheet
Norway
500 km
N
Early phase streaming (Andreassen&Winsborrow, 2009; Bjarnadóttir et al., 2013; Rüther et al., 2013)
Late phase streaming (Bjarnadóttir et al., 2013; Rüther et al., 2013)
Ice margin positions (Winsborrow, et al., 2010; Bjarnadóttir et al., 2013; Rüther et al., 2013)
3D seismic data
Extent of surfaces reconstructed from 3D seismic data
Ice dome (Dowdeswell et al., 2010)
Ice divide (Ottesen et al., 2005)
Datings:(Salvigsen, 1981; Rüther et al., 2011)
Elevation [m asl]
0
1000
Water depth [m bsl]
>500 450
0
B
Sørkapp Basin
Gardarbanken High
Sentralbanken High
Bjarmeland Platform
Hoop Fault Complex
Stappen High
Mercurius High
Nordkapp Basin
Fingerdjupet Sub-basin
Maud Basin
Norsel High
Bjørnøya Basin
Loppa High
Hammerfest Basin
Faults
Other geological boundaries
3D seismic data
Cretaceous High
Deep Cretaceous Basin
Palaeozoic High in Platform
Early Cretaceous Platform
Pre-Jurassic Basin in Platform
Shallow Cretaceous Basin
Terraces and Intra-Basin Elevations

Figure 1. (A) Bathymetric map of the study area with the reconstructed relief surface displayed as white polygon and the extent of 3D seismic data used for this reconstruction (red outline). The inset in (A) shows location of the epicontinental Barents Sea and the study area (black rectangle) displayed in Fig.1A. During the local Last Glacial Maximum (LGM) the Barents Sea Ice Sheet (BSIS) extended to the shelf break in the western Barents Sea and its limit is indicated by the white dashed line (Svendsen et al., 2004). The basemap was taken from the International Bathymetric Chart of the Arctic Ocean (IBCAO, version 3.0) (Jakobsson et al., 2012). Black and yellow arrows indicate previously inferred major ice stream directions (for early – black - and late – yellow phases of ice streaming) (Andreassen and Winsborrow, 2009; Rüther et al., 2013). Major ice domes (orange dashed lines) are suggested to have been located over NE Svalbard (Dowdeswell et al., 2010) and Storbanken (Ottesen et al., 2005). Red dashed lines show reconstructed ice margin positions during deglaciation (Bjarnadóttir et al., 2013; Rüther et al., 2013; Winsborrow et al., 2010a). Gravity cores with minimum deglaciation ages for the downstream and upstream end of Bjørnøyrenna are marked with black dots. Shaded area on the continental slope west from Bjørnøyrenna marks the extent of the Bjørnøya Trough Mouth Fan (TMF) deposited during multiple periods of ice streaming in Bjørnøyrenna. (B) Geology of the study area with structural elements including faults and other boundaries, highs, basins and platforms (NPD, 2015). The majority of the study area lies within soft, Cretaceous Bjarmeland Platform, but in the south is partly bordered by hard rocks of the Loppa and Mercurius Highs.

2.2. Glacial history and previous work

There is clear evidence for multiple glaciations of the Barents Sea during the Cenozoic, with a grounded ice sheet reaching the shelf edge at least four times (Faleide et al., 1996; Solheim and Kristoffersen, 1984; Vorren and Laberg, 1997). Throughout these periods of glaciation, Bjørnøyrenna served as the major route for BSIS discharge (Andreassen et al., 2008; Vorren and Laberg, 1997), as evidenced by the Bjørnøya Trough Mouth Fan (TMF) (Fig. 1A, shaded area). The Bjørnøya TMF constitutes a major depocenter of multiple streaming events and is the largest sedimentary fan in NW Europe, comparable in extent to the delta of Mississippi River. The total volume of 670,560 km^3 is equivalent to a 1000 m thick layer of sediments and soft Cretaceous bedrock eroded from the vast areas of SW Barents Sea (Faleide et al., 1996; Ottesen et al., 2008).

2.2.1. Barents Sea Ice Sheet (BSIS) geometry

The shoreline elevation and age records from islands surrounding the Barents Sea constituted key evidence for some of the first reconstructions of the BSIS, with the extent and geometry of the ice sheet inferred from the patterns of isobases, the magnitude of Holocene uplift on Kong Karls Land, and the geomorphology of the seabed offshore Svalbard (Boulton et al., 1982; Dowdeswell et al., 2010; Elverhøi and Solheim, 1984; Lambeck, 1995). Studies of the seabed geomorphology around Spitsbergen were used to infer the location of major ice domes over NE Svalbard and Sentralbanken (Fig. 1) (Dowdeswell et al., 2010). Ice sheet modelling of the BSIS estimated a maximum thickness of the BSIS to approach ~2000 m and velocities of 75-100 m yr^{-1} for the Bjørnøyrenna Ice Stream (Siegert and Dowdeswell, 1996). Other sources suggested ice thickness reaching 3000 m over Novaya Zemlya (Fig.2) based on raised shorelines and isostatic rebound modelling (Lambeck, 1995).

The Last Glacial Maximum for the western extent of the BSIS occurred around 21 ka BP (Landvik et al., 1998). The deglaciation of the BSIS was asynchronous (Hughes et al., 2016),

with the first stages of deglaciation in the W Barents Sea thought to coincide with the build-up and glacial maximum in the E part of the ice sheet (Demidov et al., 2006; Larsen et al., 2010). A scarcity of dates limits a precise chronology of the sub-stages during deglaciation, but the outer shelf in the SW Barents Sea was deglaciated around 18-16 ka BP (Aagaard-Sørensen et al., 2010; Rasmussen et al., 2007; Rüther, 2012). An age for the deglaciation of lower Bjørnøyrenna was estimated based on material from the outermost ice marginal sedimentary deposits identified as the 'Bjørnøyrenna end moraine zone' by Andreassen et al. (2008), and dated to 16.6-17.1 cal ka by Rüther et al. (2011) (Fig. 1A, outermost red dashed line at the Bjørnøyrenna outlet). The timing of deglaciation of upper Bjørnøyrenna is less well constrained and currently based only on raised shorelines in Kong Karls Land dated to 11.1-11.5 cal ka (Salvigsen, 1981) (Fig. 1A). The most recent reconstruction of the BSIS interpolates most of the available chronology into time slices for the entire Eurasian ice sheet growth and retreat (Hughes et al., 2016).

2.2.2. Bjørnøyrenna Ice Stream

To date, mapping of central Bjørnøyrenna has mostly been based on shallow seismic and bathymetric data (Fig. 2) which, considering the low resolution of these data compared to this study, did not allow the identification of sub-stages of Bjørnøyrenna Ice Stream retreat, or a detailed reconstruction of the ice stream behaviour (Andreassen et al., 2008; Andreassen and Winsborrow, 2009; Andreassen et al., 2014; Bjarnadóttir et al., 2014; Rüther et al., 2011; Winsborrow et al., 2010a). Nevertheless, the SW part of the Barents Sea, including the outer part of Bjørnøyrenna, has been investigated using several 2D and 3D seismic datasets. Interpretation of Late Weichselian imprints of the Bjørnøyrenna Ice Stream were performed based on industry seismic 2D and 3D datasets from the outer shelf and southern flank of Bjørnøyrenna (Andreassen et al., 2008). This included mapping of the large-scale glacial geomorphology of the seafloor and several buried surfaces (palaeo-seafloors), and documented

landforms associated with the LGM and two consecutive readvances (Andreassen et al., 2008). Further reconstructions of deglaciation included combined 2D and 3D seismic data and bathymetric data from the outer shelf of Bjørnøyrenna, which resulted in the identification of major grounding zone wedges and the reconstruction of the patterns of ice marginal deposition and the relative chronology of early phases of deglaciation (Rüther et al., 2011).

More recent studies (Fig. 2) have provided an overview of ice stream dynamics and landforms in the central part of the Barents Sea and in upper Bjørnøyrenna (Andreassen et al., 2014; Bjarnadóttir et al., 2014). Bjarnadóttir et al. (2014) established the most comprehensive reconstruction of Bjørnøyrenna Ice Stream behaviour, based on Olex dataset and IBCAO, as well as chirp and single-channel seismics. This revealed several different assemblages of bedforms indicating grounding line positions and palaeo-ice flow direction, (e.g. MSGLs and ice marginal sedimentary deposits), but did not show the details of Bjørnøyrenna Ice Stream flow variability on such short time scales.

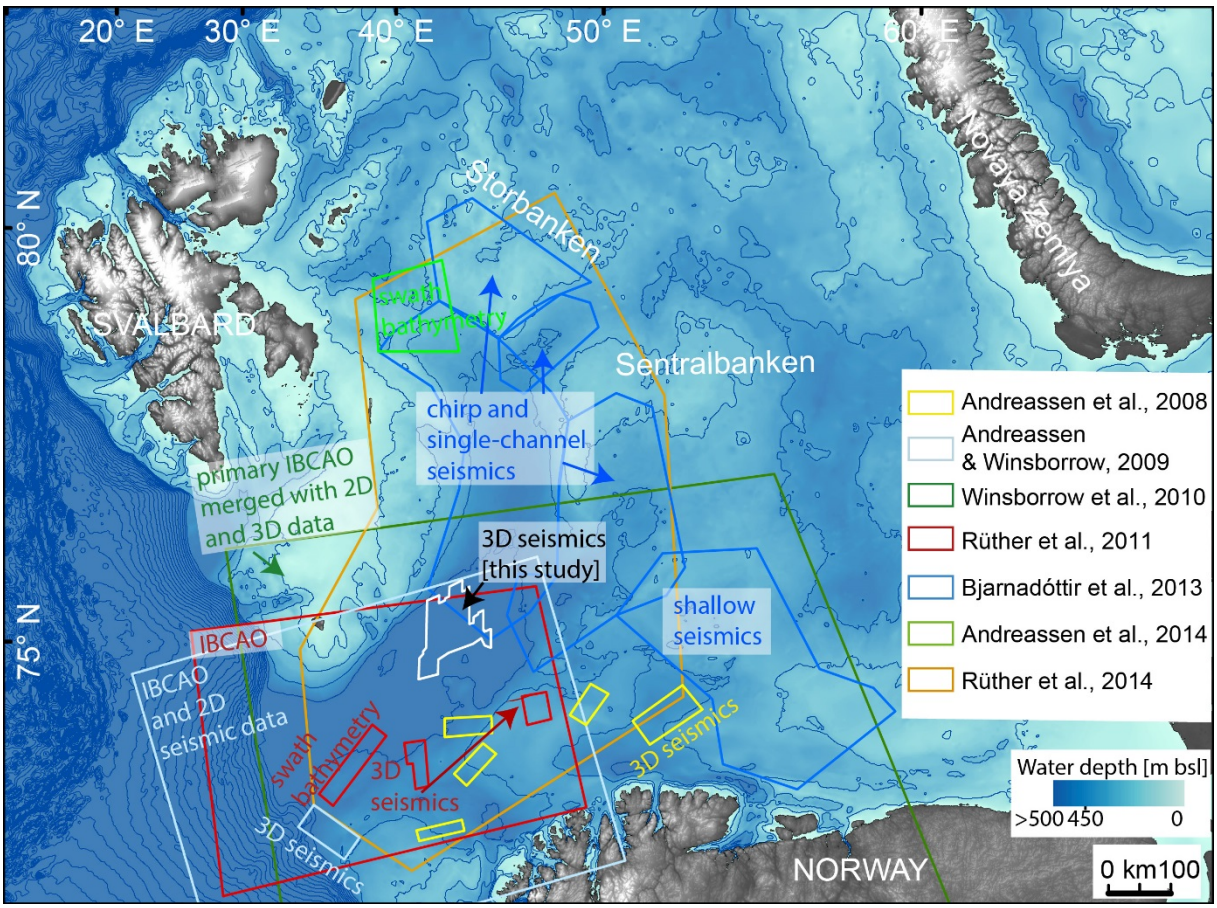

Figure 2. Regional geomorphology of the SW-central Barents Sea and a compilation of previous work on the Bjørnøyrenna Ice Stream dynamics with dataset type and extent indicated for each particular study. Background bathymetry from IBCAO v. 3.0 (Jakobsson et al., 2012). See inset in Fig. 1A for location.

180

3. Datasets and methods

We created two relief images of surfaces from merged high-resolution 3D seismic industry data covering 13,000 km^2 in central Bjørnøyrenna (Fig. 1A). The data has both vertical and horizontal resolution of 12.5 m and was provided by Statoil ASA and TGS Norway. The lower surface – the palaeo-seafloor – separates the base of glacigenic Quaternary sediments from sedimentary bedrock, which in central Bjørnøyrenna lies about 57-63 m below the present seafloor. The upper surface corresponds to the contemporary seafloor, reconstructed at the top of the glacigenic sedimentary package. Comparison of the glacial geomorphology of the two surfaces was used to map glacial geomorphology and reconstruct the time-transgressive
190 behaviour of the Bjørnøyrenna Ice Stream during deglaciation, including flow switching.

Interpretation of the 3D seismic data was performed in Schlumberger Petrel 2014. Both surfaces were reconstructed through mapping of high-amplitude reflector horizons across the extent of the seismic cube. The discontinuity of seismic horizons in the outermost parts of the 3D seismic dataset (Fig. 1A, red outline) only allowed partial reconstruction of the relief surfaces in these areas (Fig. 1A, white polygon). Due to seismic wave properties, features observed on the buried horizon and the seafloor represent a depth interval of at least a quarter of the wavelength above and below the mapped surface (which in this case is 7.5-11 m assuming the frequency of 40-60 Hz and velocity 1800 m/s) (Andreassen et al., 2008). The velocity value for two-way-travel time to depth conversion (1800 m/s for glacigenic sediments) was used after Sættem et al.

(1992). The interpreted horizons were exported and gridded to a cell size of 10 m in Fledermaus DMagic v.7. For geomorphological mapping of the landforms, ArcMap v. 10.3 was used.

3.1. Geomorphology-based inversion method

The reconstruction of Bjørnøyrenna Palaeo-Ice Stream dynamics was based on geomorphological mapping and follows the palaeo-glaciological inversion method (Hughes et al., 2014; Kleman and Applegate, 2014; Kleman and Borgström, 1996; Kleman et al., 1997; Kleman et al., 2006; Stokes et al., 2009). This method draws inferences about former ice sheet behaviour based on the geomorphological and geological record (Kleman and Borgström, 1996). The parallel alignment of geomorphological elements (usually glacial lineations) constitutes the major tool for identification and reconstruction of palaeo-ice stream flow patterns, and sediment distribution and sources (Stokes and Clark, 1999). The focus of the geomorphic mapping of the reconstructed surfaces was on highly elongate linear ridge-groove features, which were by far the most common landform. These were interpreted to be mega-scale glacial lineations (MSGLs) that consist of a ridge with two parallel lateral grooves (Clark et al., 2003). In terrestrial settings, MSGLs are usually identified and mapped based on their elongate sediment ridge (Clark et al., 2003), but this can be very difficult in marine-settings, where the initiation and the termination of the ridge can be very hard to identify (see also Spagnolo et al., 2014). Thus, we chose to map the corrugated surface based on the grooves that lie parallel to ridges, which were far more prominent and easier to identify on the seafloor and palaeo-seafloor surfaces. This likely reflects the poorer preservation potential of the ridges, as well as the very dense, crosscutting and overprinting nature of the MSGL ridges within the study area. The mapped grooves were then grouped into flow-sets (each flow-set representing a discrete ice-streaming event) using the criteria from Clark (1999):

- Parallel concordance – landforms classified according to their similar orientation,

- Similar morphometry – landforms should be of similar morphometry within the flow-set,
- Close proximity –comparable spacing between landforms from each flow-set (usually 2-3 times the width of lineation).

The length and orientation of the grooves was extracted using their start and end points. MSGL width corresponds to the width of the ridges and relief is the amplitude between the deepest point of a groove and crest of an associated ridge. Statistical frequency distribution analysis was performed using the directional vector azimuth values for each particular flow-set and plotted on a rose diagram (Fig. 7B and 8B) using Rose.NET freeware (Thompson, 2004). These diagrams show the number of occurrences of each azimuth value within a flow-set, including the bias of the value presented as 'standard deviation' (Williams, 1980).

4. Results

4.1. Large-scale morphology of palaeo-seafloor and seafloor

The study area covers 120 x 105 km within central Bjørnøyrenna (Fig. 3A). A NW-SE oriented profile (x-x') across the dataset reveals a W-shaped profile of the trough, with two shallow overdeepenings on the palaeo-seafloor and two more prominent overdeepenings on the seafloor, separated by a convex-shaped threshold (Fig. 3A, B). One large (~35 km wide and 20-50 m deep) overdeepening occurs in the north-western part of the trough in the study area, while a narrower (12 km across) but deeper one (50-70 m, relative to the flanks of the trough) occurs further to the south-east (Fig. 3B). The narrow, southern overdeepening coincides with a semi-parallel, large SSW-NNE oriented fault complex (Fig. 3C). The slopes on the flanks of the trough are gentle. The average slope gradient for the northern flank ranges from 0.15 to 0.2°, while on the southern flank it is 0.1-0.15°. Average water depth in the study area is ~400 m bsl, while in the two prominent overdeepenings depths reach 450 m in the northern part of the seafloor and 470 m to the south (Fig. 3A). Towards the south-east of the study area a shallow bank can be observed, which has been associated with a subcropping structural high (Mercurius High) where the water depths reach 400 m. The NE-SW oriented profile (y-y') shows a shallow topographic step in the upstream part of the seafloor and palaeo-seafloor, with water depths increasing towards the south-west (Fig. 3D). The SW part of the palaeo-seafloor exhibits a reversed slope (Fig. 3D). The elevation difference between the shallowest and deepest part of the palaeo-seafloor is ~60 m. The seafloor has topography inherited from the palaeo-seafloor, with a thin (60-70 m) cover of sediments in the central part (Fig. 3D).

The interpreted palaeo-seafloor (Fig. 4) lies at a depth of ~70 m under the contemporary seafloor. This surface is a clear unconformity of strong seismic amplitude, with underlying dipping sedimentary bedrock cut by overlying parallel reflectors (Fig. 3C). Seismic profiles reveal a net of polygonal faults in the sedimentary bedrock underneath the palaeo-seafloor (Fig.

4A, C). The palaeo-seafloor (Fig. 4A) is inferred to correspond to the Upper Regional Unconformity (URU) - an erosional surface that can be correlated across much of the Barents Sea, and defining the boundary between pre-glacial dipping sedimentary bedrock and overlying sediments of glacial origin (Faleide, 1996; Solheim and Kristoffersen 1984; Vorren et al., 1986). The URU surface has been eroded during repeated Quaternary glaciation cycles (Solheim and Kristoffersen 1984), which resulted in a generally thin (~70 m) sediment cover of mostly Late Weichselian origin (Faleide, et al., 1996). The bedrock and glacial debris eroded during these cycles, have been deposited in the Bjørnøya Trough Mouth Fan (Vorren and Laberg, 1997). The total erosion rate in the Barents Sea during Cenozoic was estimated to 500-2000 m (Nyland, et al., 1992). The URU is characterized by complex patterns of linear and curvilinear ridge-groove features (see section 4.2, Fig. 4A, B).

The seafloor seismic reflection (Fig. 5) shows topography inherited from URU and the surface is covered with abundant linear ridge-groove features in the eastern and central part of the area, while to the west curvilinear grooves are dominant (see section 4.2).

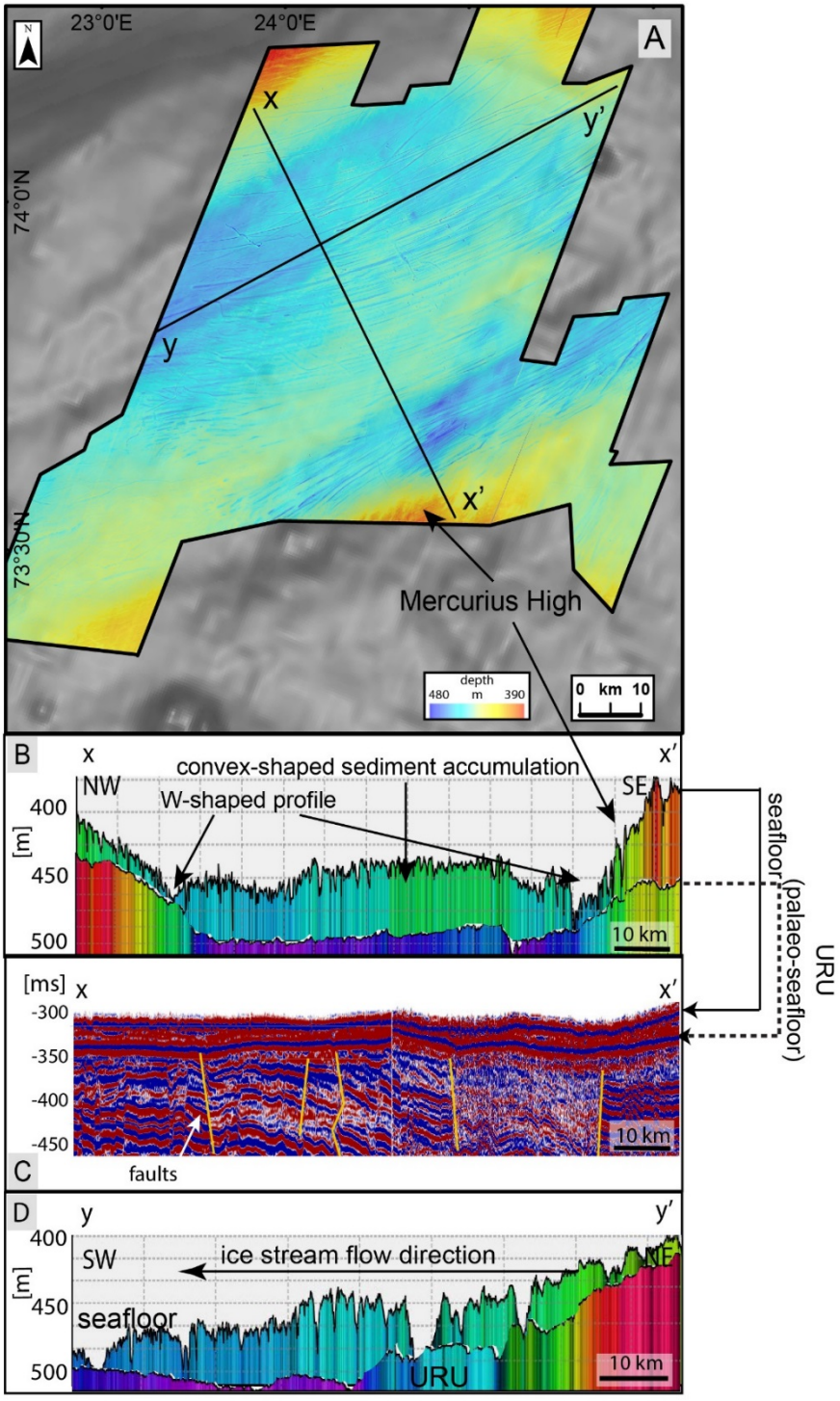

Figure 3. (A) Large-scale bathymetry of the modern seafloor in central Bjørnøyrenna. (B) Topography of the seafloor and the URU shows two overdeepenings on both surfaces and a convex-shaped sediment accumulation in the central part of the seafloor (colour-scaled to elevation). (C) Seismic profile indicating the location of the seafloor and the URU, as well as

underlying geology. Yellow vertical lines indicate major faults in the area. (D) Profile (colour-scaled to elevation) along the Bjørnøyrenna axis showing the topographic step in the NE part of the palaeo-seafloor (URU) and its reverse slope in the SE part. The seafloor topography was inherited from the palaeo-seafloor, with a convex-shaped sediment accumulation in the central part.

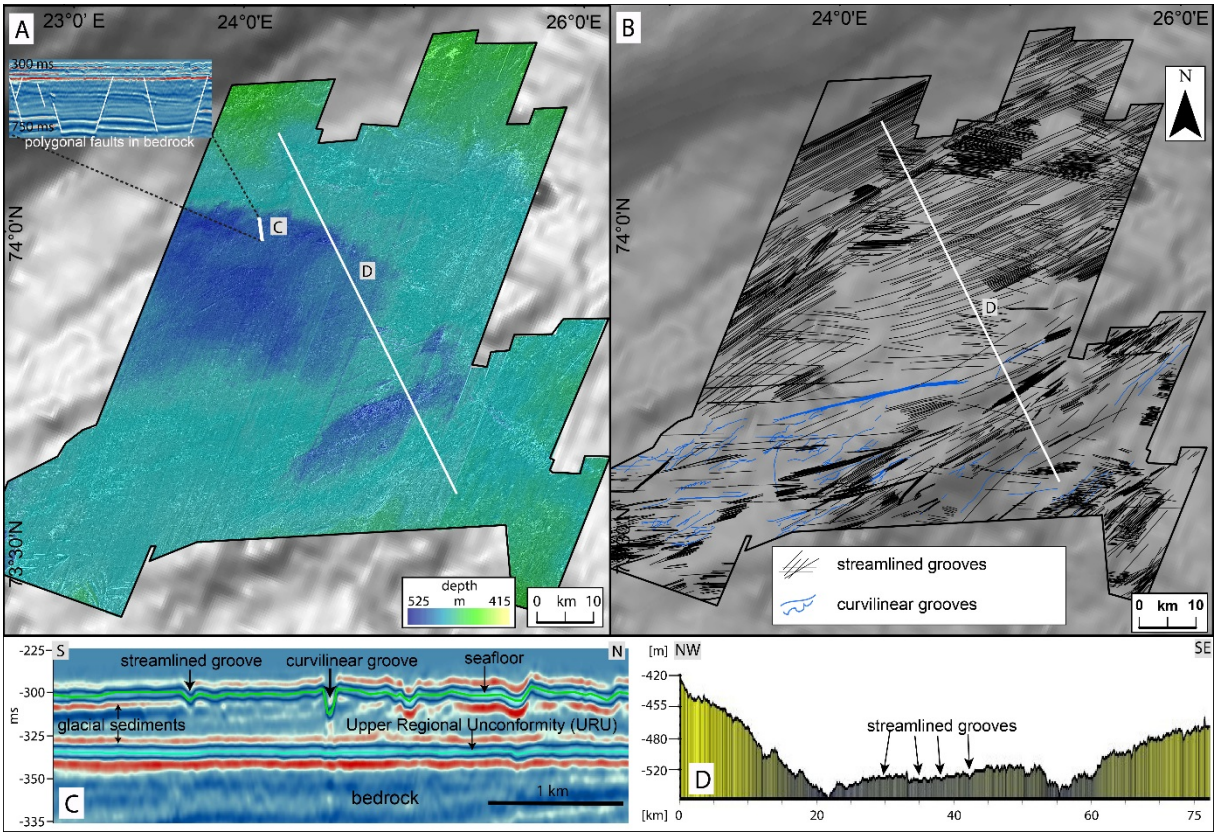

Figure 4. (A) Bathymetry of the URU. Seismic profile displays frequent polygonal faulting reaching up to the URU surface. (B) Mapping of the URU shows numerous linear (black lines) and a number of curvilinear features (blue curvilinear lines). (C) Seismic section showing two seismic horizons (surfaces): the seafloor (green) and the URU (blue), with indicated linear and curvilinear features. (D) Bathymetric cross-profile of the URU surface, with prominent W-shaped nature and numerous streamlined grooves.

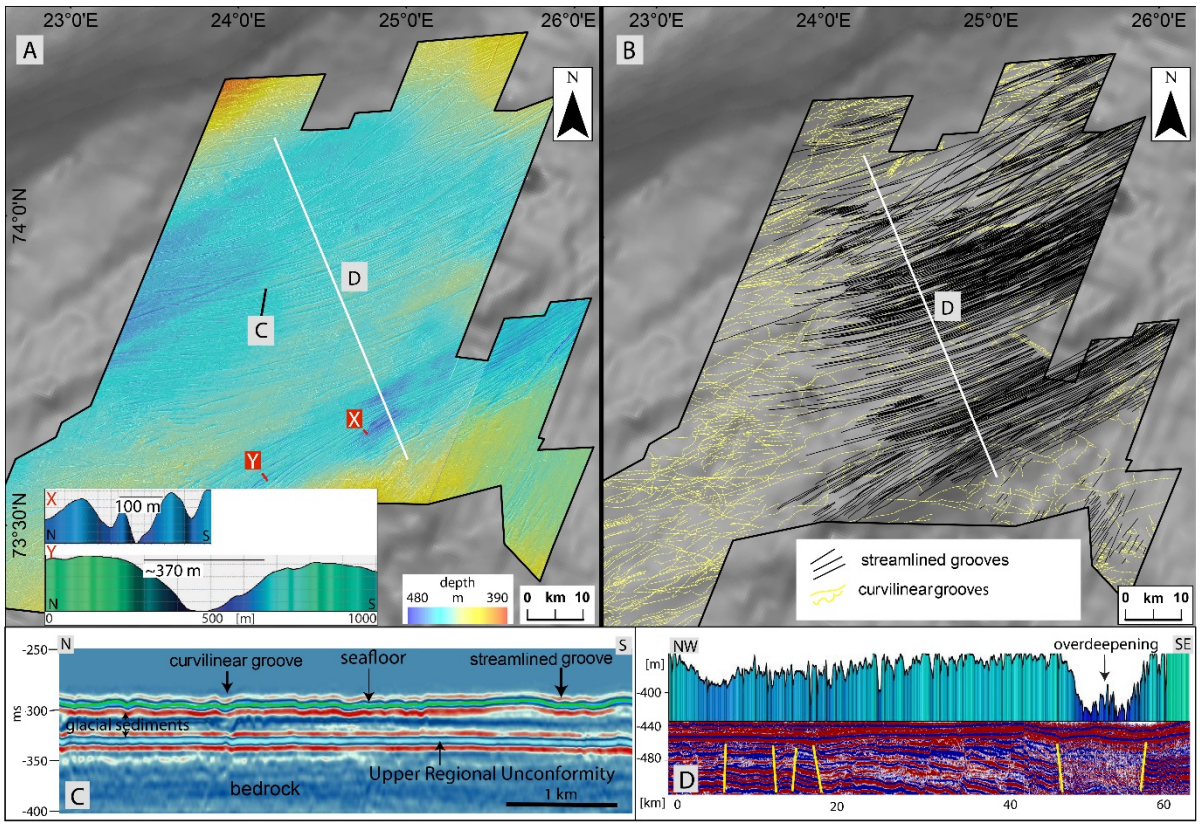

Figure 5. (A) Modern topography of the seafloor in central Bjørnøyrenna. Two overdeepenings and the elongated sediment accumulation visible in the bathymetry and profile D. (B) Geomorphological mapping of the seafloor with dominant ridge-groove composite landforms (black lines) and curvilinear grooves (yellow lines). (C) Seismic section showing two seismic horizons (surfaces): the seafloor (green) and the URU (blue), with mapped linear and curvilinear features. (D) Cross-section through the seafloor surface, showing the bathymetry with two prominent overdeepenings and numerous ridge-groove features and underlying structures. Note the large fault coinciding with the overdeepening in the south.

4.2. Small-scale geomorphology

Two main groups of glacial landforms have been identified on the URU and the contemporary seafloor: ridge-groove corrugations and curvilinear to sinuous grooves. They are described and interpreted below.

4.2.1. Curvilinear grooves

Description: Grooves of highly varying orientation and random patterns occur abundantly on the downstream part of the seafloor (Fig. 5A and 6) and in the south-western areas of the URU (Fig. 4B). Multiple grooves overprint and crosscut each other. Their width reaches 450 m and depth is up to 20 m, while the longest curvilinear groove exceeds 45 km in length. On the seafloor they occur at water depths ~400 – 450 m.

Intepretation: The curvilinear features are interpreted as iceberg ploughmarks, a product of sediment ploughing by keels of drifting icebergs. They occur downstream from the inferred ice margin and represent imprints of multiple generations of icebergs, discharged during deglaciation. Iceberg ploughmarks resembling those mapped in the study area, have been observed in numerous settings, both on modern and palaeo-continental shelves, and are typically linked to open water conditions at the ice margin (Bjarnadóttir et al., 2014; Dowdeswell et al., 2010; Dowdeswell and Ottesen, 2013; Syvitski et al., 2001).

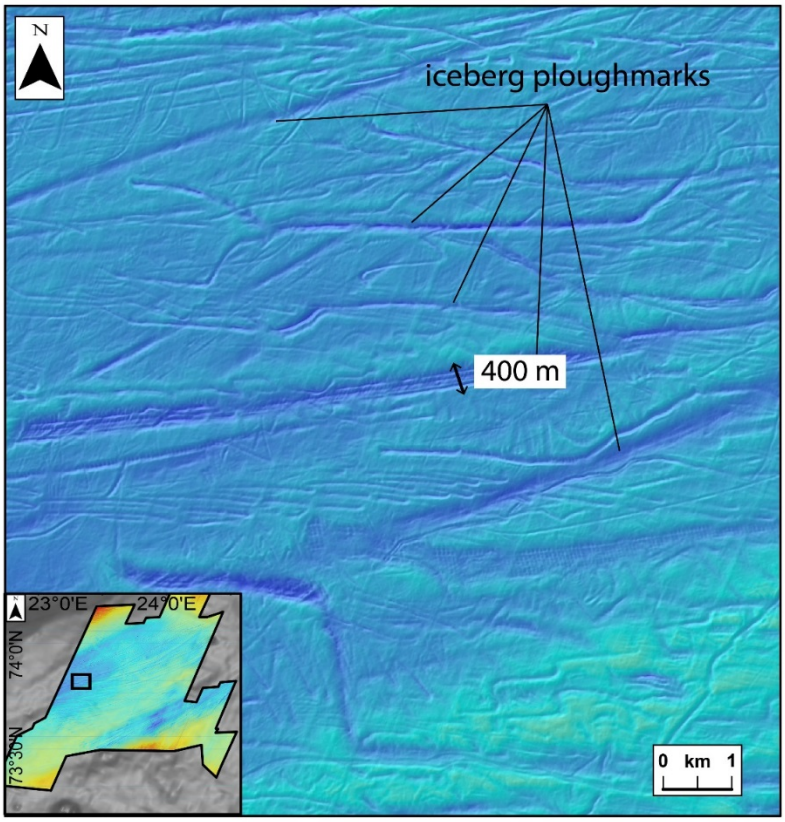

Figure 6. Examples of iceberg ploughmarks on the seafloor. They display a crosscutting and overprinting pattern with variable orientation and high sinuosity.

4.2.2. Linear ridge-groove features

Description: In total, >3500 streamlined ridge-groove features (mapped as grooves) were identified on both the URU and the seafloor. These are by far the most dominant landforms on both surfaces. Most features comprise a groove with a ridge on each side (Fig. 5A, profile X and Y), but in some cases the ridges have been eroded. The longest grooves on both surfaces reach 70 km and the width of associated ridges exceeds 700 m. The elongation ratio of the intervening ridges between grooves ranges from 50:1 to 200:1 (for details see following sections 4.3 and 4.4).

Interpretation: The mapped ridge-groove features are interpreted as assemblages of mega-scale glacial lineations (MSGLs) formed beneath fast-flowing ice (Clark, 1993). Their

morphometry is consistent with the definition of MSGLs – parallel ridge-groove corrugations of 6-100 km in length and characterised by elongation ratios 2-200:1. They resemble numerous other examples of MSGLs mapped on beds of palaeo-ice streams in different settings (Clark, 1993; King et al., 2009; Spagnolo et al., 2014).

The MSGLs have been interpreted to record the activity of the former Bjørnøyrenna Ice-Stream (e.g. Andreassen and Winsborrow, 2009). The multiple sets of cross-cutting lineations reported in this paper indicate several generations of ice streaming. Using the criteria from Clark (1993), the mapped grooves were grouped into 10 distinct flow-sets (see section 3.1 for methods), with 5 on each surface (the URU and seafloor).

We interpret each population to represent a different phase of ice-stream flow, separated in time. Based on the crosscutting relationship, the relative chronology of the streaming events were reconstructed, although the precise age is uncertain. In the following section, we document and describe the ice stream flow-sets and their relative chronology.

4.3. Ice stream flow-sets 1-5: URU (palaeo-seafloor)

The mapping of the URU reveals 2,630 individual grooves, covering the extent of the surface (Fig. 4B, 7A). Their length varies from ~0.3 km to ~70 km and the longest groove extends almost across the whole URU surface (~70 km). The width of the ridges between adjacent grooves varies from 100 to ~360 m and they are up to 6 m in relief. The grooves exhibit a widely varying orientation, from E-W oriented to NNE-SSW oriented (Fig. 7B). The relative chronology, inferred from crosscutting and overprinting relationship between the mapped grooves on URU is presented in Figure 7 and will be discussed below.

4.3.1. Flow-set 1

The lowermost flow-set 1 is overprinted by streamlined features from flow-sets 2, 3, 4 and 5 and is, therefore, interpreted as the oldest assemblage of streamlined grooves, which

covers the whole URU surface (Figs. 7A, C). Grooves forming this flow-set are oriented E to W, diverging (increasing spacing) towards the west and curving slightly towards WNW. The entire MSGL assemblage (flow-set) has a maximum length of 105 km and width of almost 90 km, but we infer it has much larger extent, given its likely extension beyond the studied surface. The longest groove of this flow-set is 37 km long, but the mean length is less than 6 km. The width of the ridges does not exceed 260 m and their relief is 3-4 m at maximum.

4.3.2. Flow-set 2

The second oldest flow-set documents flow towards the SSW and occurs exclusively in the south-easternmost part of the dataset (Figs. 7A, C and D). The relative age of this flow-set is based on the cross-cutting relationship between flow-set 2, 3 and 5. Flow-set 2 is restricted to the SE part of the URU and has a width of about 20 km, while its length extends for over 30 km at minimum, but it likely exceeds dimensions of the study area to the south (Fig. 7A). Individual grooves have varying dimensions, with lengths ranging from very short (several hundreds of meters) to approximately 30-35 km. The relief of the ridges varies within the range of 1 to 7 m and their width ranges from 100-250 m.

4.3.3. Flow-set 3

The third streaming event flow-set can be observed along the axis of the narrow overdeepening in the southern part of the URU, continuing towards the SW, diverging and changing direction to WSW further downstream (Figs. 7A, D, E). Flow-set 3 overprints flow-set 1 and underlies flow-set 4. The width of this flow-set varies from 10 km in the narrow overdeepening, to 25 km downstream, where the lineations diverge; while the length reaches over 110 km. Individual grooves are not well preserved, but regularly and closely distributed, and are most apparent in the area of the overdeepening. Their lengths vary from 0.5-34 km and the width of associated ridges ranges from 200 to ~350 m, while the relief is 0.5-5 m on average.

4.3.4. Flow-set 4

Similar to flow-sets 2 and 3, this SW oriented assemblage (Figs. 7A, E, F) can only be mapped over restricted areas in the western part of the URU and in the overdeepening, but it has a uniform distribution of lineations with a relatively regular spacing. Flow-set 4 overprints flow-set 3, and underlies flow-set 5. The width of this flow-set is approximately 60 km and the total length exceeds 65 km. The length of individual grooves varies from 0.6 to over 30 km, the width of the ridges mostly exceeds 200 m and their relief reaches up to 5 m.

4.3.5. Flow-set 5

This is the uppermost assemblage of grooves, related to the youngest streaming event on the URU surface (Figs. 7A, F). In the north-easternmost part of the surface, the flow-set is WSW oriented and grooves have a regular spacing, but converge slightly westwards. This flow-set is superimposed on flow-set 4. The width of this flow-set is approximately 40 km and its length exceeds 70 km. Grooves of this assemblage have lengths varying from ~10 km to over 70 km, while the width or the ridges ranges from 100-250 m. The relief of the ridges in this flow-set ranges from 1-5 m.

4.4. Ice stream flow-sets 6-10: modern seafloor

Mapping of the modern seafloor reveals ~900 individual grooves, covering most of the upstream part of the seafloor surface (Figs. 8A). The ridge-groove features create dense patterns of crosscutting and overprinting bedforms, varying in orientation and dimensions. The length of the grooves varies from 10 km to ~70 km. The intervening ridges are 100-700 m wide and have relief from 2 m up to 15 m. The grooves are WSW to SSW oriented (Fig. 8B). The relative chronology of the streaming events is presented in Figure 8 and is based on crosscutting and overprinting relationship between the seafloor flow-sets.

4.4.1. Flow-set 6

The lowermost flow-set on the seafloor consists of several long, wide and widely spaced grooves (Figs. 8A, C). It is present in the upstream part of the seafloor and oriented WSW. Flow-set 6 was inferred to be the oldest flow-set on the seafloor, based on its crosscutting relationship with flow-set 7. The width of this assemblage is ~30 km and length is ~40 km. The length of individual grooves ranges from ~10 to over 70 km, while the width of the ridges varies from ~200 to 500 m. The vertical relief of the ridges ranges from 2 m to 8 m.

4.4.2. Flow-set 7

This flow-set crosscuts flow-set 6 at a low angle and consists of widely spaced grooves (Figs. 8A, C and D). The assemblage is SW oriented and is seen only in the upstream area of the seafloor. Flow-set 7 extends about 30 km in width across the shallow upper areas of the seafloor and has length of about 60 km. The length of individual grooves varies from ~10 km to 50 km, the width of the ridges varies between 150-300 m and their relief ranges from 2 m to 7 m.

4.4.3. Flow-set 8

This is the most extensive flow-set on the seafloor and covers the whole eastern and central part of the seafloor (Figs. 8A, D and E). Flow-set 8 is WSW oriented and overprints flow-set 7 in the northern part of the seafloor and underlies flow-set 9 in the south. The flow-set curves slightly towards the west and, to the south, is bordered by the overdeepening occupied by flow-set 9. This assemblage is 60 km wide and ~60 km long. Grooves within this flow-set are densely spaced and have a minimum length range of 25-55 km, with many extending beyond the study area. The intervening ridges have widths ranging from 200-500 m, and a relief of 2 to 10 m.

4.4.4. Flow-set 9

This is a narrow flow-set and, similarly to flow-set 3 on URU, is focused along the structural overdeepening in the south of the study area (Fig. 8A, E and F). The flow-set is oriented SW, slightly changing direction in its downstream part towards SSW. It overprints flow-set 8 in the northern flank of the overdeepening and is cross-cut by flow-set 10 in the upstream part. The flow-set is ~70 km in length and over 10 km in width. The convergent pattern of the grooves in this flow-set is most prominent in the narrow overdeepening in the southern part of the seafloor, where the grooves are narrower and more closely spaced. Outside the overdeepening, the grooves diverge, forming a lobate shape. Individual grooves have lengths varying from several to almost 60 km, the intervening ridges vary in width from ~100 to > 700 m and have a relief ranging from 2 m to 15 m.

4.4.5. Flow-set 10

This is the uppermost (youngest) flow-set on the seafloor, and occurs exclusively in the south-easternmost part of the surface (Fig. 8A, F). Due to the cross-cutting relationship with flow-set 9, it was inferred to be the youngest assemblage on the seafloor. This assemblage is oriented SSW and consists of a small number of short, widely spaced grooves, extending over an area of about 30 km in length and ~30 km in width. The streamlined features within the flow-set 10 have lengths varying from ~1 km to ~14 km, while the width of the ridges ranges from ~100 m to almost 600 m. Their relief varies from 2 to 10 m.

5. Discussion

5.1. How many streaming events were there and how did the streaming direction change during deglaciation?

In this study we identified ten flow-sets in Bjørnøyrenna (Figs. 7 and 8), significantly more than has been identified in previous studies, which had suggested up to three flow sets in central Bjørnøyrenna, all of which were likely associated with the deglaciation (Andreassen et al., 2008; Andreassen and Winsborrow, 2009; Bjarnadóttir et al., 2014; Rüther et al., 2011; Winsborrow et al., 2010a). The modern seafloor flow-sets identified in this study, partly correlate with the deglaciation flow-sets proposed by other authors with regard to their extent and orientation (ranging from SSW in Bjarnadóttir et al. (2014) to WSW in e.g. Andreassen et al. (2008) and Winsborrow et al. (2010a). However, the data used in this study, demonstrate much larger variations in the trajectory of the Bjørnøyrenna Ice Stream, with ten differently oriented flow-sets identified. We interpret these flow-sets to represent ten ice streaming events separated in time (five on the paleo-seafloor surface – URU, and five on the modern seafloor). The varying orientation and extent of these streaming events documents the dynamic behaviour of the ice streams operating in Bjørnøyrenna, which we now discuss.

5.1.1. URU

Flow-set 1 is the first evidence of ice streaming sourced directly from the east of Bjørnøyrenna (Fig. 7A and 9). The fragmentary character of these lineations and their length and shallow depth are consistent with the notion that they represent the oldest assemblage, with the nature of the substrate (bedrock) allowing for partial preservation of the grooves. The streaming event can be mapped across the whole interpreted horizon and likely extends beyond the study area. Its orientation across the Bjørnøyrenna trough, independent of the large scale topography, indicates prolonged fast ice-flow within an ice sheet of large thickness during maximum style glaciation. This is consistent with the results of a new numerical model of the

BSIS-SIS (Fig. 13) and is most likely to correlate with greater ice sheet thicknesses around the time of the Last Glacial Maximum (~21 ka BP). Indeed, maximum ice thickness during the LGM has been estimated to 2-3 km (Forman et al., 1995; Landvik et al., 1998; Patton et al., 2016, in review), which is an order of magnitude greater than topographic variations around the study area in Bjørnøyrenna. For example, the elevation difference between shallow banks in the central part of the Barents Sea and Bjørnøyrenna is about 300 m (compare section 2.1), which is significantly less than the estimated LGM ice thickness and, as such, would not have provided a significant topographic barrier to ice flow. Flow-set 1 is therefore an ice streaming event associated with topographically independent (pure) flow across a hard bed; a 'rigid-bed ice stream' (Eyles et al., 2016; Kleman et al., 2006; Krabbendam et al., 2015; Stokes et al., 2009), it is significantly different from the subsequent flow sets 2-10, and inferred to represent maximum-type glaciation.

Flow-set 2 is interpreted to have occurred after a significant period of time (likely millennial time scale) relative to flow-set 1, based on the large differences in the extent and orientation between flow-sets 1 and 2 (Figs. 7 and 9, flow-set 2). Flow-set 2 is much smaller in extent than the oldest flow-set 1 and occurs only in the SE part of the dataset. Based on the small differences in extent and orientation, we interpret the time interval between flow-sets 2 and 3, and flow-sets 4 and 5 to be relatively short (centennial time scales). Using the terminology of Kleman and Borgström (1996), flow-sets 2-5 likely represent ephemeral ice streams.

The topographically constrained character of flow-sets 2-5 (confined to the area of Bjørnøyrenna) suggests rapid thinning of the ice sheet. Flow-set 2 is only seen in the SE part of the URU and displays a significantly different, SSW orientation than flow-set 1 (Figs. 7A, B and 9). Given the large change in ice flow direction between flow-sets 1 and 2 we suggest that flow-set 2 was formed during the initial rapid retreat of the ice sheet from its maximum shelf edge position. This initial retreat could have been followed by subsequent period of ice margin

stabilization and associated deposition of the grounding zone system in outer Bjørnøyrenna identified in Winsborrow (2010) and further dated to ~16.5-17.1 ka BP by Rüther et al. (2011). The third ice streaming event (flow-set 3) is narrow and topographically-constrained (Figs. 7 and 9), and likely following one of the topographic overdeepenings within the trough (Fig. 10). Flow-sets 4 and 5 indicate a shift in streaming direction towards the SW. Their extent is wider than the flow-sets 2-3 (Figs. 7A and 9), suggesting that the ice stream occupied a major part of Bjørnøyrenna at this time. It is likely that these events represent a re-advance followed by further ice margin retreat and are tentatively correlated with the maximum ice extent for 16 ka BP (Hughes et al., 2016).

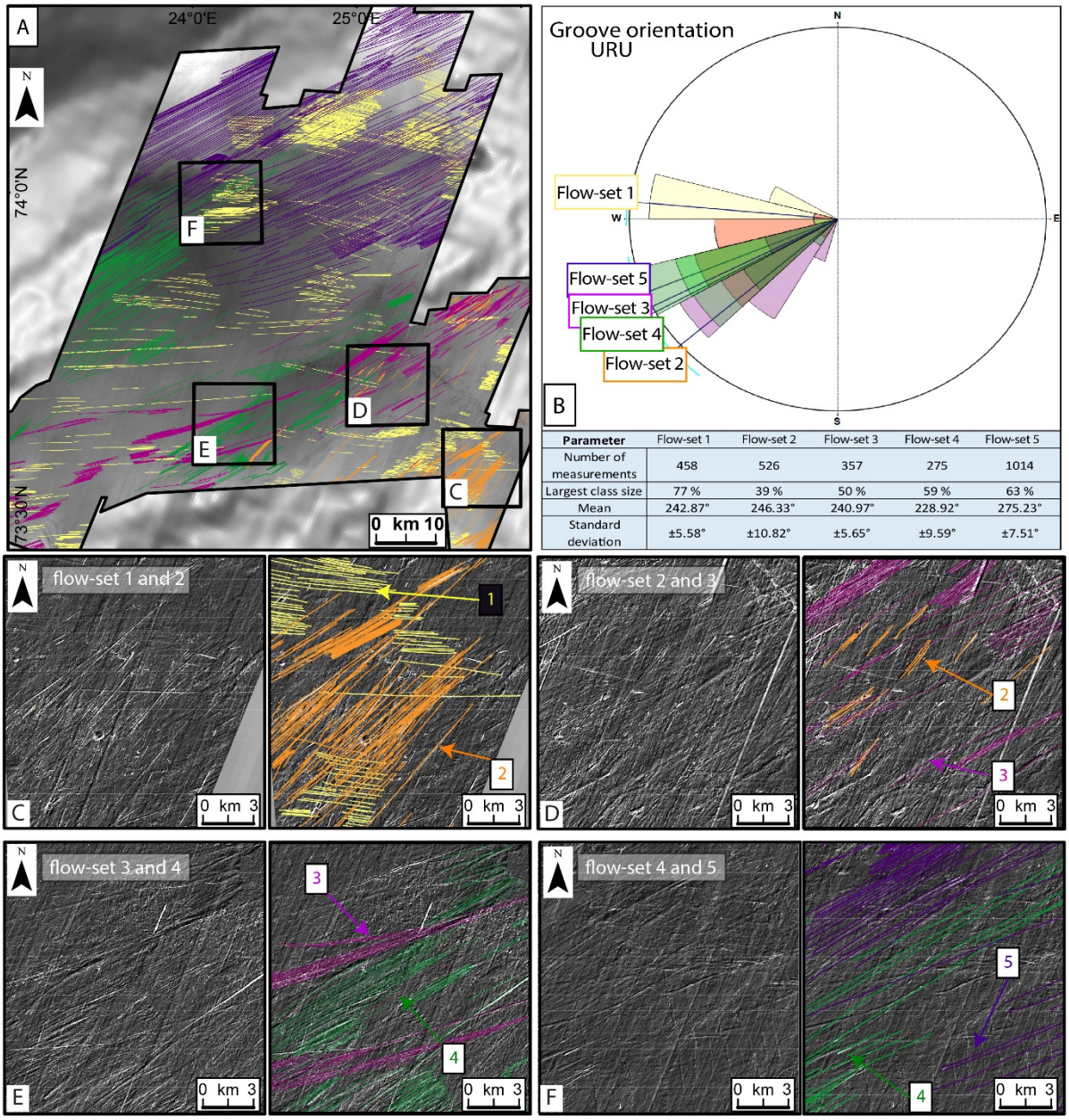

Parameter	Flow-set 1	Flow-set 2	Flow-set 3	Flow-set 4	Flow-set 5
Number of measurements	458	526	357	275	1014
Largest class size	77 %	39 %	50 %	59 %	63 %
Mean	242.87°	246.33°	240.97°	228.92°	275.23°
Standard deviation	±5.58°	±10.82°	±5.65°	±9.59°	±7.51°

Figure 7. (A) Streamlined ridge-groove features on the URU were classified into five different streaming events and numbered 1-5 with different colours, from the lowermost (oldest) to the uppermost (youngest). Crosscutting relationships are shown in zoom-in figures (C-F). (B) Rose diagram showing the varying orientation of streaming events (in relative chronological order) on the buried surface in central Bjørnøyrenna indicating flow switching from W to SSW.

5.1.2. Seafloor

The seafloor displays a significantly different pattern of streaming than the URU (Fig. 8 and 11) and is represented by different characteristics of ridge-groove features (MSGLs). The MSGLs on the contemporary seafloor comprise prominent, relatively continuous ridges and grooves, which are longer, deeper and have higher relief compared to URU flow-sets. Their elongation ratio (>100:1) and parallel conformity over long distances might indicate higher ice-flow velocities during formation of these lineations (Clark, 1993; Stokes et al., 2013) or it may simply reflect their more complete preservation. The upstream part of the seafloor is covered mostly by streamlined bedforms, while the downstream part of the area is dominated by iceberg ploughmarks (Figs. 5B and 6). In contrast to the URU, switching in the streaming direction on the seafloor occurs in counter-clockwise manner (compare Fig. 9 and 11), which we interpret as reflecting the migration of the ice dome and the ice divide northwards (see also section 5.2). The grooves in flow-sets 6-10 display a high variability in orientation and, in some cases (flow-set 7-9) have convergent, curved flow patterns. Moreover, within these flow-sets, it is possible to infer tentative ice-stream grounding line positions, based on the assumption that the termination of MSGLs and initiation of ploughmarks represents the transition from the subglacial to the proglacial domain (Fig. 8A).

At least nine ice stream marginal positions were identified in Bjørnøyrenna by Bjarnadóttir et al. (2014) immediately upstream of the study area and were interpreted to represent a highly dynamic system with periodic ice stream slowdown, stagnation and re-advance. We interpret flow-sets 6-10 to represent similar cycles of ice-stream slowdown and re-advance during deglaciation (suggested to be between 17-15 ka BP based on the reconstruction of Hughes et al. (2016)). Hughes et al. (2016) suggested a probable separation of Scandinavian Ice Sheet and Svalbard-Barents-Kara Ice Sheet (SIS and SBKIS, respectively) around this time, and other authors have also suggested multiple ice-margin oscillations associated with the overall retreat

and detachment of SBKIS from the SIS (Rüther, 2012). The oldest streaming imprints on the seafloor (flow-set 6: Fig. 8A and 11) are seen only in the upstream part of the trough, and are oriented towards the SW with a relatively narrow extent. The termination of these lineations in the center of the trough is interpreted to represent the ice stream grounding line at the time of their formation. We suggest that this event can be associated with topographically constrained retreat along Bjørnøyrenna, following separation of SBKIS and SIS (Hughes et al., 2015; Winsborrow et al., 2010). Flow-sets 7 and 8 (Fig. 8B and 11) show a switch in ice-flow direction towards the WSW, consistent with progressive ice sheet retreat in the SW Barents Sea (e.g. Bjarnadóttir et al., 2014; Winsborrow et al., 2010). Streaming during the events 7 and 8 occurred along wide parts of the trough, suggesting gradual thinning and widening of the ice stream lobe. Flow-set 9 (Figs. 8A, 10, 11) documents SW oriented ice streaming event along a narrow topographic overdeepening in the southern part of the seafloor, coinciding with a semi-parallel, SSW-NNE oriented large fault and structural change in bedrock. Flow-set 10 reveals streaming terminating in the inferred subcropping bedrock area (the Mercurius High) south of the overdeepening occupied by flow-set 9 (Figs. 8A and 10). The morphometry (short landforms, shallow and widely spaced) of flow-set 10 perhaps reflects a reduction in ice streaming velocities over the rough bed and against the positive slope gradient in the SE part of the seafloor. Both flow-sets 9 and 10 are inferred to represent minor ice-stream re-advances.

To summarise, we identify 10 flow-sets that represent distinct streaming events in Bjørnøyrenna and the trajectories of each of them is related to a switch in the source area (see section 5.2). Five of these appear on the palaeo-seafloor of the URU and the oldest of these (flow set 1) indicates initial ice streaming from an ice dome in the eastern part of the Barents Sea during maximum style glaciation (likely around the LGM). The flow-trajectory gradually migrated from streaming sourced from the E towards streaming sourced from the NE and became progressively more influenced by topography. The five streaming events on the modern

seafloor are interpreted to reflect further phases of episodic ice streaming during deglaciation, associated with progressive ice thinning and flow dependent on underlying topography. The direction of ice flow migrated from sourced from the NE towards ice sourced from the N.

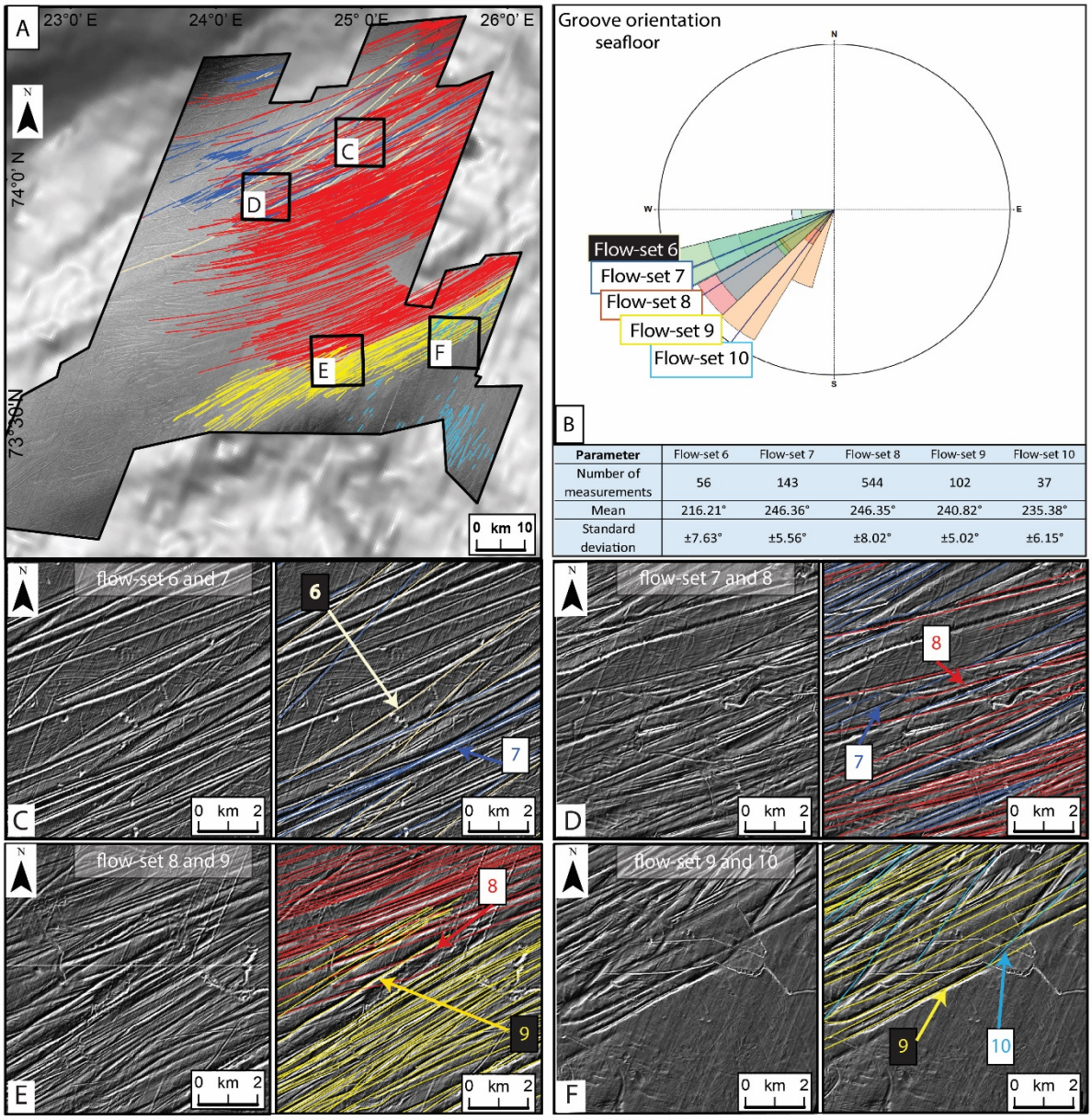

Figure 8. Five flow-sets of the modern seafloor and their relative chronology based on crosscutting relationship (C-F). (B) Frequency distribution diagram showing orientation of the flow-sets.

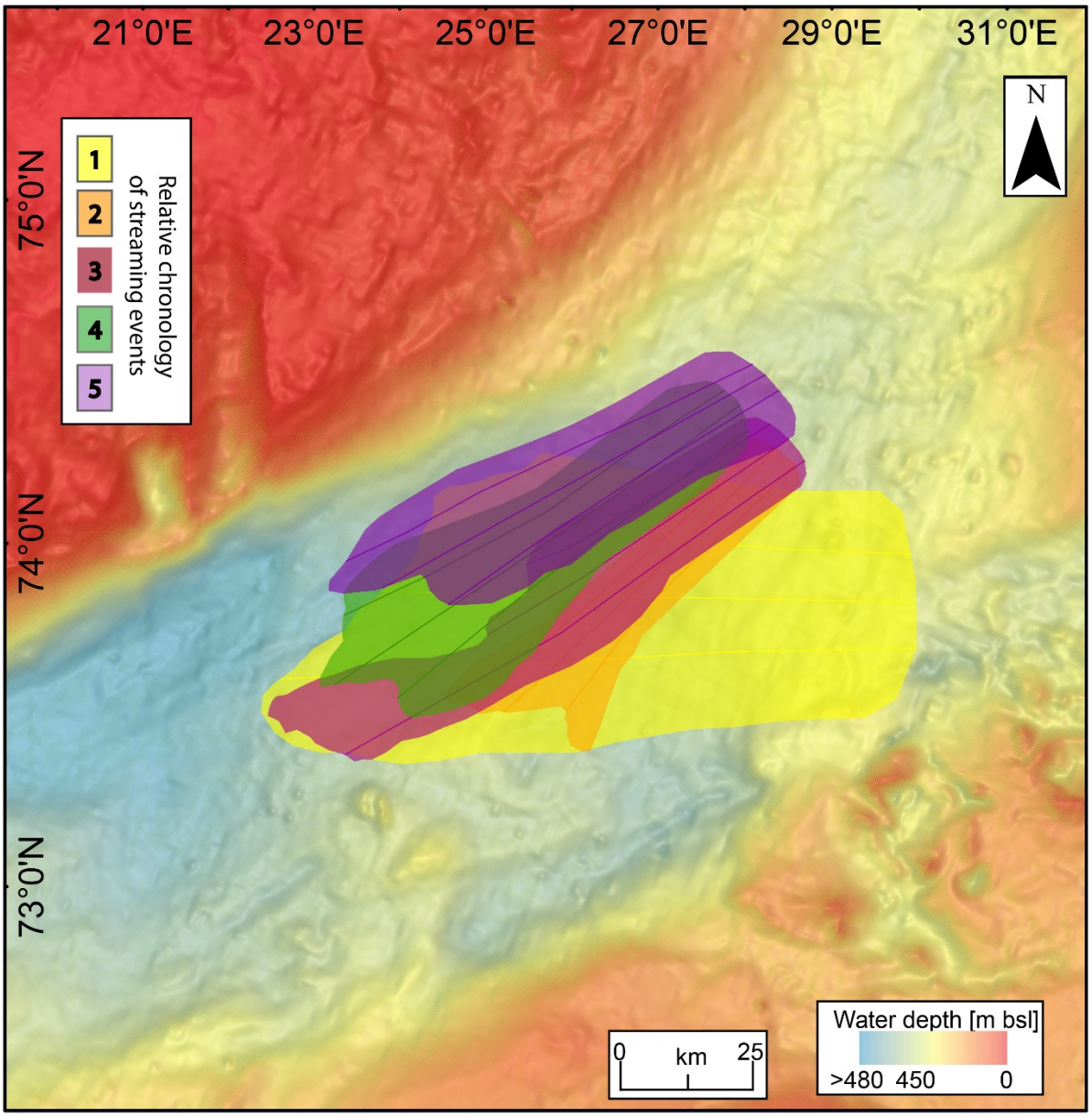

Figure 9. Schematic illustration of ice stream flow switching from the full glaciation (1) through to the mid-phase of deglaciation (5), based on ridge-groove streamlined features on the palaeo-seafloor. A regional interpretation of the extent of the streaming events is presented in Figure 12. Background bathymetry from IBCAO (Jakobsson, et al., 2012).

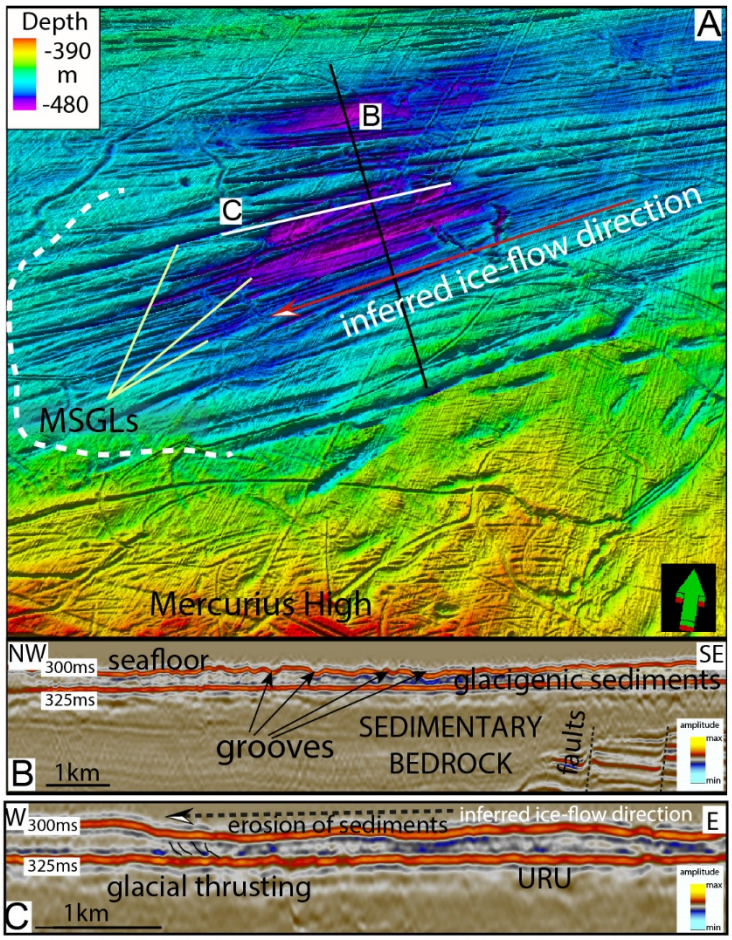

Figure 10. Example of grooves of flow-set 9 in the narrow overdeepening in the southern part of the seafloor. Profile C shows erosion of the surface and thrusting of the glacigenic sediments underneath the ice stream. The MSGLs assemblage (flow-set 9) visible in the overdeepening terminate sharply, forming a lobe (white dashed line). The shallow area of draped bedrock in the southern part constitutes a lateral flank of the flow-set and correlates with fault complex visible in SE in profile B.

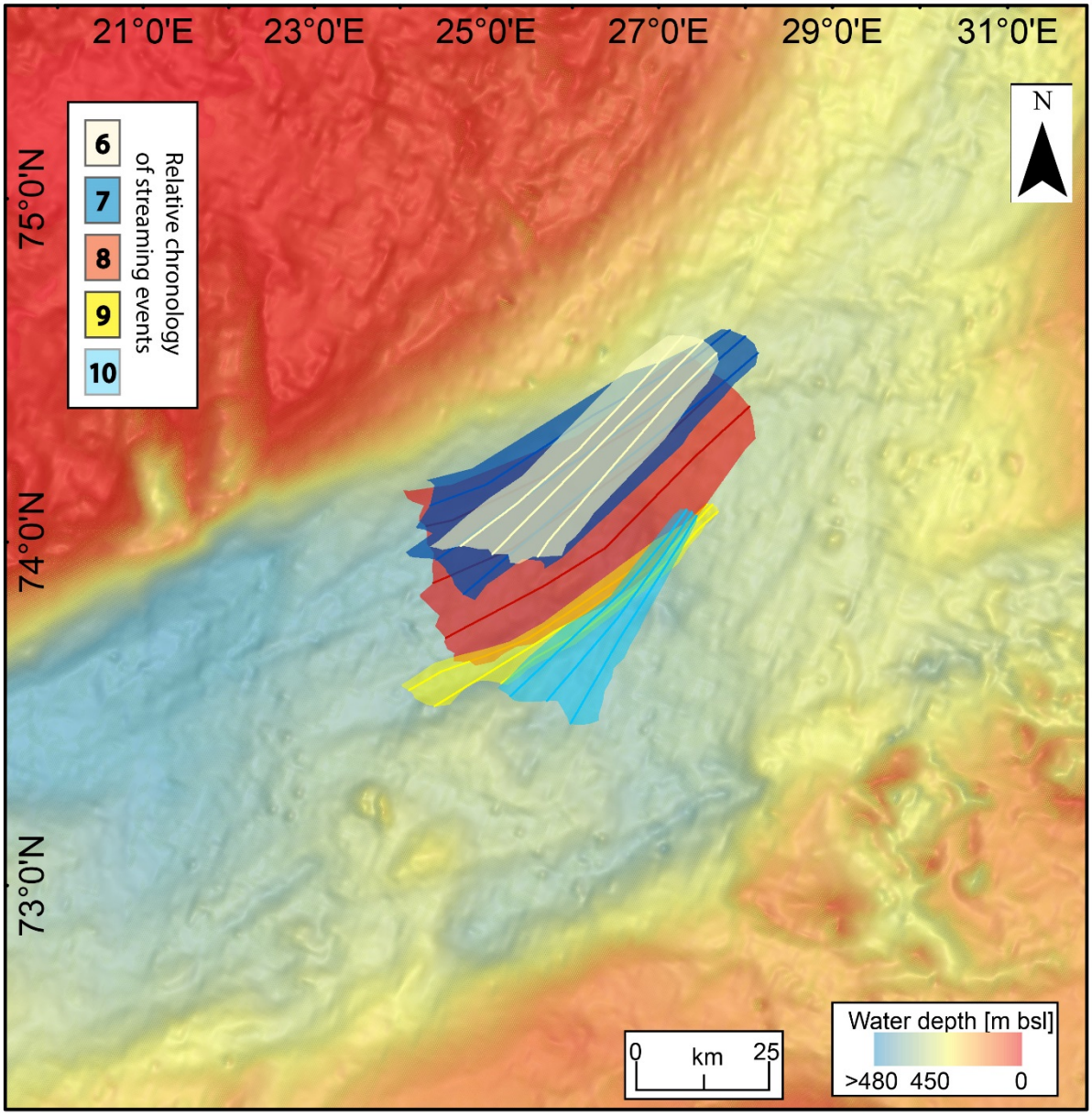

Figure 11. Ice stream flow switching during the mid-late phase of deglaciation, tentatively estimated to occur between 17 ka BP and 15 ka BP (6 oldest; 10 youngest).

5.2. Where were the major ice domes and divides located and how did they migrate through the deglaciation?

The location and dynamics of ice domes (major high elevation accumulation zones of the ice sheet and source areas for the ice streams) and ice divides (boundary areas within the ice sheet separating ice flow of opposite direction) within the BSIS have been subjects of debate for the last few decades (Andreassen et al., 2004; Andreassen et al., 2014; Bjarnadóttir et al., 2014; Hogan et al., 2010; Ingólfsson and Landvik, 2013; Lambeck, 1995; Landvik et al., 1998; Ottesen et al., 2005; Patton et al., 2015; Rüther et al., 2012; Svendsen et al., 2004; Vorren et al., 2011; Winsborrow et al., 2011). Previous reconstructions have generally portrayed major ice domes over Novaya Zemlya, with estimated ice thickness up to 1.75 km (Siegert et al., 2001), and over Storbanken High and Kong Karls Land (estimated ice thickness of 1,5-2 km) (Dowdeswell et al., 2010; Lambeck, 1995; Lambeck, 1996; Ottesen et al., 2005) or east of Kong Karls Land (Forman, 2004). Our observations of changes in ice stream trajectory allow us to reconstruct the likely location of major ice domes that fed the ice stream events during deglaciation from the LGM to about ~15 ka BP (Fig. 12). This reconstruction is based on the relative chronology of Bjørnøyrenna ice stream flow-sets 1-to-10 identified in this study, combined with the ice margin reconstruction of Hughes et al. (2016). On this basis, we show the highly dynamic nature of the multi-domed BSIS, with LGM ice domes located considerably further east than has been suggested previously.

Stage 1 (flow set 1) (Fig. 12A) is dominated by an E-W oriented flow-set that clearly indicates a large ice stream draining into the western, outer part of Bjørnøyrenna, from a dome in the east, south-east of Sentralbanken (Fig. 12A, D1). This is the first time that the main centre of ice mass during a maximum-style glaciation, like the LGM, has been suggested to be located so far. This empirically-based interpretation is, however, consistent with the most recent numerical modelling of the BSIS from Auriac et al. (2016) and Patton et al. (2016, in review)

(Fig. 13). Ice streaming during this event was not topographically constrained, indicating significant ice thicknesses. During the LGM, the dome existing in the north-east (Fig. 12 A, D2) proposed by Lambeck (1996) and Forman et al., (2004) had little influence on ice discharge in the SW Barents Sea. Instead this dome fed ice northwards through the Kvitøya and Franz Victoria Troughs (Fig.12). We suggest that the BSIS and SIS were coalescent during this period and we therefore reconstruct an ice divide running broadly N-S along the centre of the BSIS, connecting these two ice domes (Fig. 12A). Compared to previous reconstructions (Dowdeswell et al., 2010; Ottesen et al., 2005; Winsborrow et al., 2010a) the southern ice divide (Fig. 12, D1) is shifted significantly eastwards, increasing the drainage area towards the south-western BSIS margin. As such, existing estimates of glacial erosion rates in the SW Barents Sea, based on a more limited drainage area (Laberg et al., 2011), may need to be revised.

Stages 2 and 3 (flow sets 2-3) are tentatively associated with the grounding zone wedge complex in SW Bjørnøyrenna, dated to approximately 17 ka BP (Fig. 12B) (Andreassen et al., 2008; Rüther et al., 2011). During that period, a significant portion of the south-western Barents Sea has been deglaciated (Rüther et al., 2011; Winsborrow et al., 2010a). A significant shift in orientation of the ice stream compared to Stage 1 is consistent with major and rapid migration of the source areas: towards the south-west in the case of the northern dome, and towards the north-west in the case of the southern dome. This implies a displacement of these source areas of about 150 km between the LGM and ~17 ka BP and an ice margin retreat of around 120 km. This is also associated with a significant reduction in the catchment area of the Bjørnøyrenna Ice Stream compared with the LGM.

Stages 4 and 5 (flow sets 4-5) have been correlated with the 16 ka BP ice margin and represent a minor re-advance of the ice stream during overall retreat of the BSIS (Fig. 12C). The advance may have occurred due to internal instabilities of the ice sheet during the separation of the BSIS from the SIS, as suggested by Hughes et al. (2016). Interpretation of streaming directions

identified in our data, suggests a slight shift in the ice divides southwards, as well as gradual thinning of the ice and, hence, the ice domes.

Continued retreat during stage 6 (flow set 6) caused progressive migration of the northern ice dome towards the south, whilst the southern dome was now migrating towards Sentralbanken (Fig. 12D). The streaming events (flow sets) 7 and 8 suggest a highly unstable ice sheet, characterised by several re-advances (oscillations) of the ice stream margin (Fig. 12E, Stage 7 and 8). We interpret the BSIS and SIS to destabilise around the southern border of the ice divide at that time.

Stages 9 and 10 (flow sets 9-10) depict another minor re-advance of the ice stream and migration of the source areas slightly to the north-west (Fig. 12F). We suggest the major source area for stage 10 to be located over Storbanken, while the southern ice divide center was interpreted to play a minor role for the topographically driven ice flow along Bjørnøyrenna during the final stage (around 15 ka BP).

In summary, we interpret the BSIS to be a multi-domed ice sheet, with the LGM ice divide located farther to the south-east than previously suggested. Furthermore, we document significantly larger and more frequent shifts in ice sources from one streaming event to another compared to previous reconstructions, with ice dome migration of up to 150 km between full style glaciation (stage 1) and mid-deglaciation (stage 10).

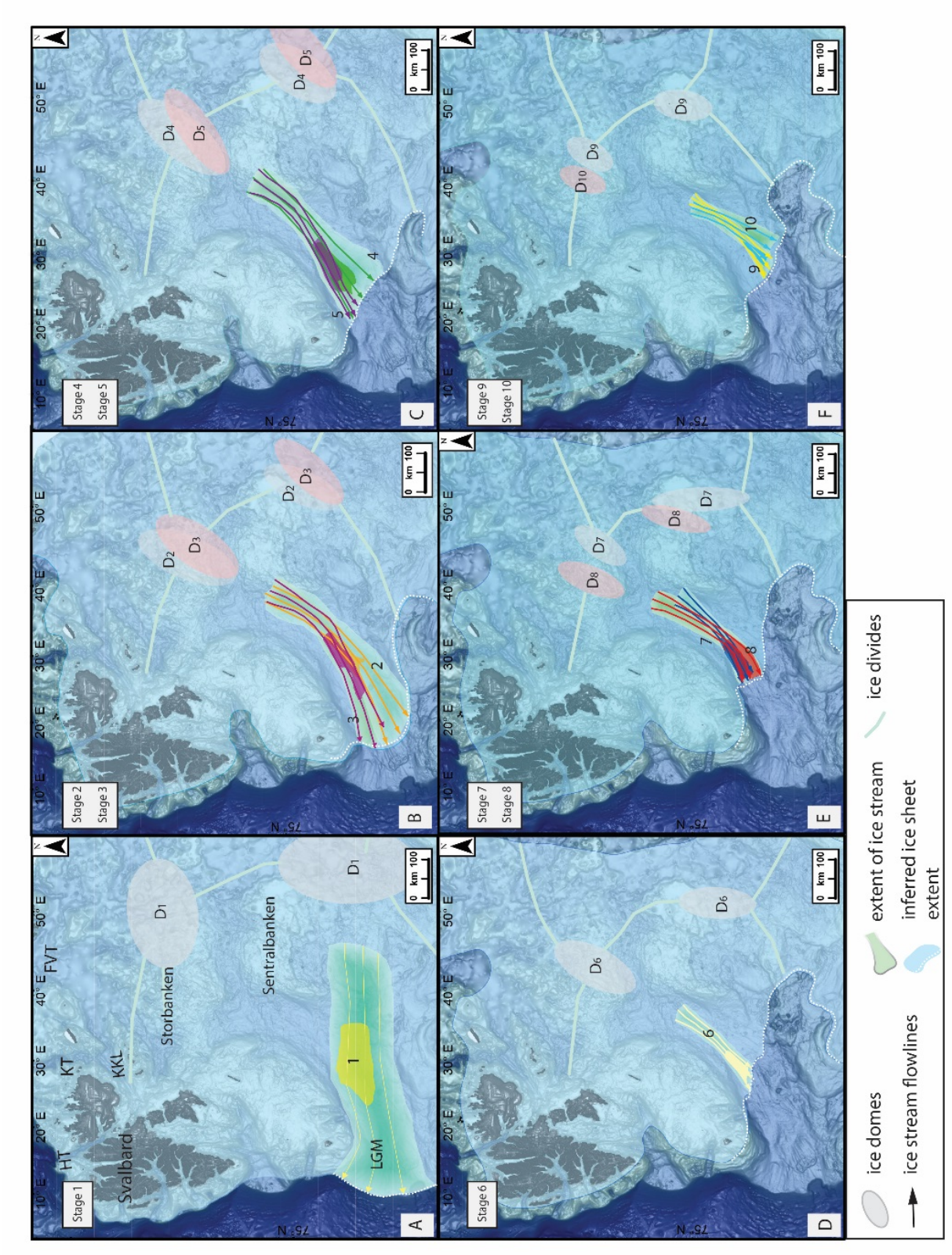

Figure 12. Stepwise reconstruction of the SW Barents Sea Ice Sheet deglaciation from maximum-style glaciation like the Last Glacial Maximum to mid-deglaciation, showing

frequent changes in trajectory and extent of identified flowsets and associated ice divides migration. The extent of ice streaming was inferred based on the interpreted ice stream flowlines and the extent of MSGL assemblages. The BSIS extent is from Hughes et al., (2015), with ice margins in Bjørnøyrenna adjusted to the extent of flow-sets identified in this study; background bathymetry from IBCAO (Jakobsson et al., 2012). Abbreviations: HT – Hinlopen Trough, KT – Kvitøya Trough, FVT – Franz Victoria Trough.

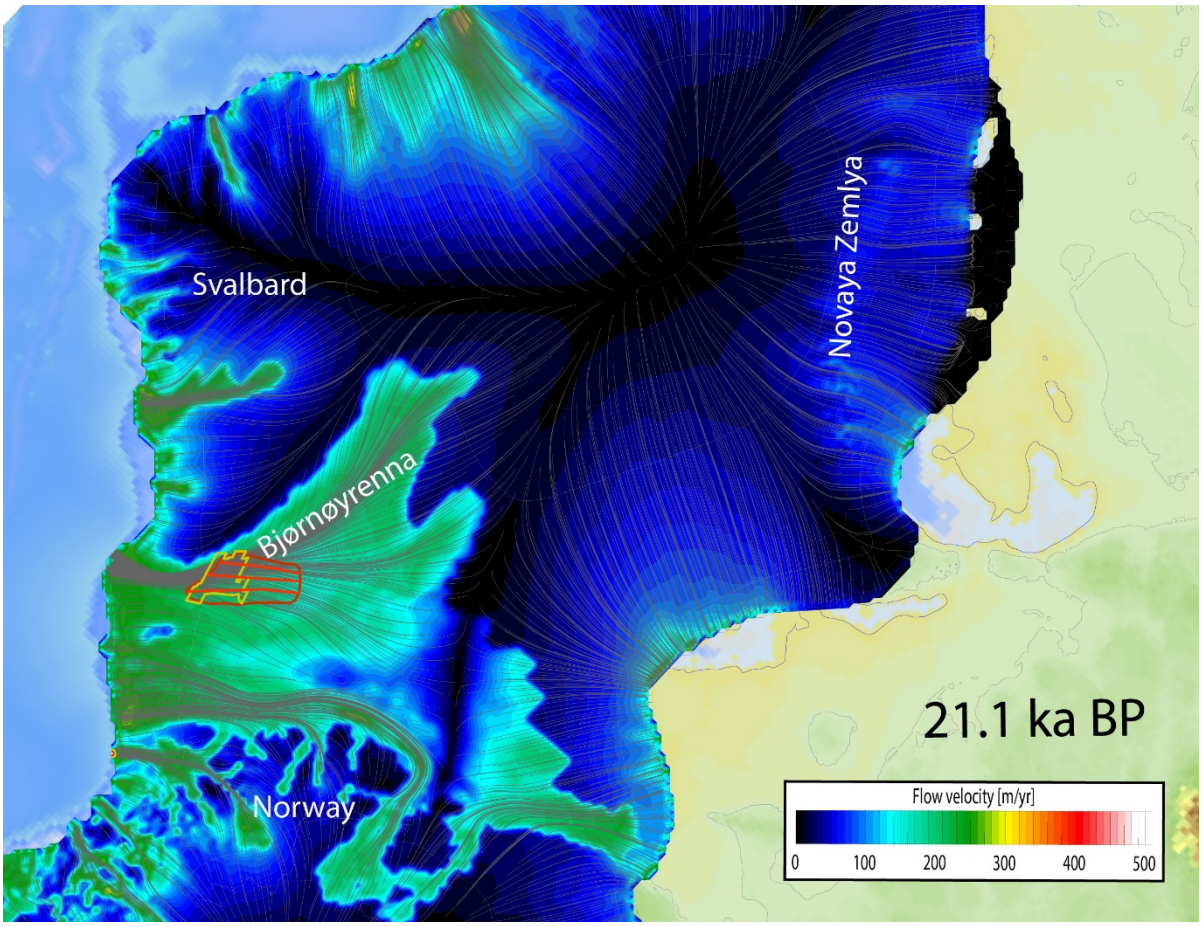

Figure 13. LGM time slice from recent 3D numerical modelling of the BSIS-SIS (Patton et al., 2016, in review), showing the flow orientation and velocities of the Bjørnøyrenna Ice Stream. The location of our study area is indicated by a yellow polygon, with the inferred maximum glaciation flow-set extent in red. Results from this numerical model have been implemented in glacioisostatic adjustment modelling for the BSIS (Auriac et al., 2016) and correspond well to relative sea-level data.

5.3. What were the controls behind the Bjørnøyrenna Ice Stream flow switching?

This study has presented geomorphological evidence for multiple periods of flow switching of the Bjørnøyrenna Ice Stream and associated ice divides (Fig. 12 B-F). Based on previous work (Dowdeswell et al., 2006; Gregoire et al., 2012; Jamieson et al., 2012; Winsborrow et al., 2010b), we suggest that the following factors may have played a role in controlling the observed flow switching: changes in BSIS geometry (migration of the ice divides), bed topography/bathymetry and associated changes in calving at the ice margin.

We suggest that the primary control on ice stream flow switching in central Bjørnøyrenna was changes in the geometry of the BSIS, associated with shifts in the location of major ice domes and divides, as well as ice thickness. Such reorganization of the ice sheet geometry would cause shifts in the orientation of ice streaming, as the ice stream source areas migrate. Competition between adjacent source areas could have caused a slow-down of ice streaming from one source area and a gradual development of a differently oriented adjacent ice stream, discharging ice from a new source area. Primarily, these changes in the ice divides were driven by changes in ice sheet mass balance (negative mass balance leading to ice sheet thinning) in a warming climate, in addition to non-linear feedbacks. For example, changes in geometry could have been amplified by gradual destabilization of the ice divide during the detachment of BSIS from the SIS (collapse of a saddle between these two ice masses). This process is similar to the ice 'saddle' collapse mechanism suggested for Laurentide (LIS) and Cordilleran (CIS) Ice Sheets by Gregoire et al. (2012). The collapse of the saddle could have increased surface melting rates due to lowering of the general ice surface and initiated enhanced calving at the ice stream terminus until the ice sheet reaches a new equilibrium geometry (Gregoire et al., 2012).

The degree to which ice stream location is topographically steered is closely related to ice sheet thickness, with the importance of bed topography increasing as the ice sheet thins. At a broad

scale, streaming events 2-10 were located within the topographic confines of Bjørnøyrenna, which constituted the main path for the streaming (Siegert and Dowdeswell, 1996). However, evidence shows that the position of each event within the trough varied, perhaps suggesting a smaller scale topographic influence on streaming location, similar to topographic steering of ice streams in the British-Irish Ice Sheet described by Phillips et al. (2010). This is the case for the streaming events 3 and 9, 2 and 10, as well as 4 and 8. Streaming events 3 and 9 show clear topographic steering, flowing convergently along the narrow structural overdeepening which coincides with the obliquely oriented Hoop Fault Complex (Figs. 1B). Streaming events 4 and 8 occupy much of the trough, but are restricted laterally to the south by the structurally-controlled change in topography associated with Hoop Fault Complex (Figs. 7A and 9A), suggesting a topographic control on this margin. Flow-sets 2 and 10 terminate on the Mercurius High (Figs. 3A, B and 10), an elevated area of rough subcropping bedrock in the SW part of the study area, with a positive slope oriented against the inferred ice flow direction, which would have impeded the ice flow. These examples emphasise the importance of subglacial topography and bedrock structures in influencing ice stream flow.

Related to topography, variations in calving may also influence ice stream flow switching. Enhanced calving may be triggered by changes in grounding line bathymetry as the ice stream retreated along reverse bed slope towards deeper water in the central part of Bjørnøyrenna (Jamieson et al., 2012; Joughin and Alley, 2011; Polyak et al., 1997; Winsborrow et al., 2011). Indeed, the bathymetric profile along the central Bjørnøyrenna, shows a difference of up to 60 m between the shallowest and the deepest point (Fig. 3D), which could have had large implications for calving rates during the youngest streaming event (flow-set 5) on the palaeo-seafloor and the following events (flow-sets 6-9) on the seafloor. These flow-sets terminate in the deepest part of the study area, suggesting potential instabilities at the ice margin and high calving rates (Kleman and Applegate, 2014; Schoof, 2007). In this scenario, the ice mass

drawdown (and hence the ice flow velocity) was highest when the ice stream terminated in the deeper part of the trough. As it retreated towards the shallower areas in north-eastern part of central Bjørnøyrenna the ice stream could have been periodically stabilised. Such marine-terminating, reverse slope ice streams are far more sensitive to sea level variations and changes in ice properties than terrestrial terminating ice streams (Joughin and Alley, 2011; Schoof, 2007). The rapid ice mass loss could have contributed to surface lowering and ice margin retreat during later phases of deglaciation, associated with a significant reorganization of the ice sheet geometry.

In summary, we propose that the observed flow switching was triggered primarily by changes in overall ice sheet geometry and associated ice divides migration, and could have been modulated, both regionally and locally, by changes in subglacial topography. Furthermore, the flow switching could have been caused by higher calving rates due to grounding line oscillations as the ice stream retreated along the deepest parts of the trough.

6. Conclusions

- Extensive mapping of the previously undocumented central part of Bjørnøyrenna Ice Stream bed shows multiple assemblages of ridge-groove features interpreted as mega-scale glacial lineations on the present-day seafloor and a paleo-seafloor surface. The cross-cutting relationship of these landfoms allows the reconstruction of relative chronology of the streaming events and the flow variability of the ice streaming events through time.
- Five streaming events have been identified for the palaeo-seafloor and five on the modern seafloor, which implies significantly more variability in ice stream flow than previously suggested and dynamic changes in ice sheet geometry.

- We identify two types of ice streaming: pure, non-topographically constrained during maximum-style glaciation, like the LGM (Stage 1); ephemeral and locally variable deglacial ice streaming events (Stages 2-10).
- We show the first evidence of E-W oriented ice streaming during LGM-style glaciation, which is well in agreement with the new numerical modelling of the BSIS-SIS (Patton et al., 2016, in review), suggesting the presence of an ice dome shifted much further towards south-east compared to previous reconstructions. The ice catchment area would therefore increase significantly, having implications for erosion rate estimates in the south-western Barents Sea.
- We demonstrate that the ice flow in Bjørnøyrenna displayed complex temporal and spatial variations from one stage to another. The streaming occurred on different timescales, ranging from extensive, millennial-scale ice flow during LGM-style glaciation and locally variable flow on probably smaller, centennial scales during deglaciation. The direction of Bjørnøyrenna ice streaming varied broadly from W to SSW oriented, which implies large shifts in ice divide positions.
- The trajectory and vigour of the ice flow within Bjørnøyrenna Ice Stream was likely driven by externally triggered changes in geometry of the Barents Sea Ice Sheet (associated with migration of ice divides and perhaps the saddle collapse), and by variations in topography/bathymetry and associated calving of the ice stream front.

The former Barents Sea Ice Sheet constitutes an invaluable geological analogue for modern West Antarctic Ice Sheet, due to their similarities such as bed type and size during the Last Glacial Maximum. Empirical evidence obtained through analysis of geophysical datasets from the Barents Sea is important for constraining numerical models of marine-terminating, contemporary ice sheets, with respect to their future behaviour - flow variability and rates of

deglaciation. This study shows that ice streams are highly dynamic over centennial to millennial time-scales and that their flow trajectory and extent can change drastically within these time-scales, which is likely associated with changes in ice divides, with a possibility of non-linear behaviour in the system.

Acknowledgements:

This work is a contribution to “Glaciated North Atlantic Margins” (GLANAM) Initial Training Network funded by the European Community's 7th Framework Programme FP7 2007/2013, Marie-Curie Actions, under Grant Agreement No. 317217. It is also a part of ”CAGE” – “the Centre for Arctic Gas Hydrate, Environment and Climate”, supported by the Research Council of Norway through its Centres of Excellence funding scheme grant No. 223259. The 3D seismic datasets were kindly provided by Statoil ASA and TGS Norway. We thank the Editor and an anonymous reviewer for their comments during the peer review process.

References:

Aagaard-Sørensen, S., Husum, K., Hald, M., Knies, J., 2010. Paleoceanographic development in the SW Barents Sea during the Late Weichselian–Early Holocene transition. Quaternary Science Reviews 29, 3442-3456.

Andreassen, K., Nilssen, L.C., Rafaelsen, B., Kuilman, L., 2004. Three-dimensional seismic data from the Barents Sea margin reveal evidence of past ice streams and their dynamics. Geology 32, 729.

Andreassen, K., Laberg, J.S., Vorren, T.O., 2008. Seafloor geomorphology of the SW Barents Sea and its glaci-dynamic implications. Geomorphology 97, 157-177.

Andreassen, K., Winsborrow, M., 2009. Signature of ice streaming in Bjørnøyrenna, Polar North Atlantic, through the Pleistocene and implications for ice-stream dynamics. Annals of Glaciology 50, 17-26.

Andreassen, K., Winsborrow, M.C.M., Bjarnadóttir, L.R., Rüther, D.C., 2014. Ice stream retreat dynamics inferred from an assemblage of landforms in the northern Barents Sea. Quaternary Science Reviews 92, 246-257.

Auriac, A., Whitehouse, P.L., Bentley, M.J., Patton, H., Lloyd, J.M., Hubbard, A., 2016, in press. Glacial isostatic adjustment associated with the Barents Sea ice sheet: a modelling inter-comparison. Quaternary Science Reviews.

Bjarnadóttir, L.R., Rüther, D.C., Winsborrow, M.C.M., Andreassen, K., 2013. Grounding-line dynamics during the last deglaciation of Kveithola, W Barents Sea, as revealed by seabed geomorphology and shallow seismic stratigraphy. Boreas 42, 84-107.

Bjarnadóttir, L.R., Winsborrow, M.C.M., Andreassen, K., 2014. Deglaciation of the central Barents Sea. Quaternary Science Reviews 92, 208-226.

Boulton, G.S., Baldwin, C.T., Peacock, J.D., McCabe, A.M., Miller, G., Jarvis, J., Horsefield, B., Worsley, P., Eyles, N., Chroston, P.N., Day, T.E., Gibbard, P., Hare, P.E., von Brunn, V., 1982. A glacio-isostatic facies model and amino acid stratigraphy for late Quaternary events in Spitsbergen and the Arctic. Nature 298, 437-441.

Clark, C.D., 1993. Mega-scale glacial lineations and cross-cutting ice-flow landforms. Earth Surface Processes and Landforms 18, 1-29.

Clark, C.D., 1999. Glaciodynamic context of subglacial bedform generation and preservation. Annals of Glaciology 28, 23-32.

Clark, C.D., Tulaczyk, S., Stokes, C.R., Canals, M., 2003. A groove-ploughing theory for the production of mega-scale glacial lineations, and implications for ice-stream mechanics. Journal of Glaciology 49, 240-256.

Demidov, I., Houmark-Nielsen, M., Kjær, K., Larsen, E., 2006. The last Scandinavian Ice Sheet in northwestern Russia: ice flow patterns and decay dynamics. Boreas 35, 425-443.

Dowdeswell, J.A., Ottesen, D., Rise, L., 2006. Flow switching and large-scale deposition by ice streams draining former ice sheets. Geology 34, 313.

Dowdeswell, J.A., Hogan, K.A., Evans, J., Noormets, R., Cofaigh, C.O., Ottesen, D., 2010. Past ice-sheet flow east of Svalbard inferred from streamlined subglacial landforms. Geology 38, 163-166.

Dowdeswell, J.A., Ottesen, D., 2013. Buried iceberg ploughmarks in the early Quaternary sediments of the central North Sea: A two-million year record of glacial influence from 3D seismic data. Marine Geology 344, 1-9.

Elverhøi, A., Solheim, A., 1984. Barents Sea ice sheet - a sedimentological discussion. Polar Research 1, 23-42.

Eyles, N., Putkinen, N., Sookhan, S., Arbelaez-Moreno, L., 2016. Erosional origin of drumlins and megaridges. Sedimentary Geology 338, 2-23.

Faleide, J.I., Solheim, A., Fiedler, A., Hjelstuen, B.O., Andersen, E.S., Vanneste, K., 1996. Late Cenozoic evolution of the Barents Sea-Svalbard continental margin. Global and Planetary Change 12, 53-74.

Fiedler, A., Faleide, J.I., 1996. Cenozoic sedimentation along the southwestern Barents Sea margin in relation to uplift and erosion of the shelf. Global and Planetary Change 12, 75-93.

Forman, S., Lubinski, D., Miller, G., Snyder, J., Matishov, G., Korsun, S., Myslivets, V., 1995. Postglacial emergence and distribution of Late Weichselian ice-sheet loads in the northern Barents and Kara seas, Russia. Geology 23, 113-116.

Forman, S., 2004. A review of postglacial emergence on Svalbard, Franz Josef Land and Novaya Zemlya, northern Eurasia. Quaternary Science Reviews 23, 1391-1434.

Golledge, N.R., Kowalewski, D.E., Naish, T.R., Levy, R.H., Fogwill, C.J., Gasson, E.G.W., 2015. The multi-millennial Antarctic commitment to future sea-level rise. Nature 526, 421-425.

Gregoire, L.J., Payne, A.J., Valdes, P.J., 2012. Deglacial rapid sea level rises caused by ice-sheet saddle collapses. Nature 487, 219-222.

Hogan, K.A., Dowdeswell, J.A., Noormets, R., Evans, J., Ó Cofaigh, C., 2010. Evidence for full-glacial flow and retreat of the Late Weichselian Ice Sheet from the waters around Kong Karls Land, eastern Svalbard. Quaternary Science Reviews 29, 3563-3582.

Hughes, A.L.C., Clark, C.D., Jordan, C.J., 2014. Flow-pattern evolution of the last British Ice Sheet. Quaternary Science Reviews 89, 148-168.

Hughes, A.L.C., Gyllencreutz, R., Lohne, Ø.S., Mangerud, J., Svendsen, J.I., 2016. The last Eurasian ice sheets – a chronological database and time-slice reconstruction, DATED-1. Boreas 45, 1-45.

Ingólfsson, Ó., Landvik, J.Y., 2013. The Svalbard–Barents Sea ice-sheet – Historical, current and future perspectives. Quaternary Science Reviews 64, 33-60.

Jakobsson, M., Mayer, L., Coakley, B., Dowdeswell, J.A., Forbes, S., Fridman, B., Hodnesdal, H., Noormets, R., Pedersen, R., Rebesco, M., Schenke, H.W., Zarayskaya, Y., Accettella, D., Armstrong, A., Anderson, R.M., Bienhoff, P., Camerlenghi, A., Church, I., Edwards, M., Gardner, J.V., Hall, J.K., Hell, B., Hestvik, O.B., Kristoffersen, Y., Marcussen, C., Mohammad, R., Mosher, D., Nghiem, S.V., Pedrosa, M.T., Travaglini, P.G., Weatherall, P., 2012. The International Bathymetric Chart of the Arctic Ocean (IBCAO) Version 3.0. Geophysical Research Letters 39.

Jakobsson, M., Andreassen, K., Bjarnadóttir, L.R., Dove, D., Dowdeswell, J.A., England, J.H., Funder, S., Hogan, K., Ingólfsson, Ó., Jennings, A., Krog Larsen, N., Kirchner, N., Landvik, J.Y., Mayer, L., Mikkelsen, N., Möller, P., Niessen, F., Nilsson, J., O'Regan, M., Polyak, L., Nørgaard-Pedersen, N., Stein, R., 2014. Arctic Ocean glacial history. Quaternary Science Reviews 92, 40-67.

Jamieson, S.S.R., Vieli, A., Livingstone, S.J., Cofaigh, C.Ó., Stokes, C., Hillenbrand, C.-D., Dowdeswell, J.A., 2012. Ice-stream stability on a reverse bed slope. Nature Geoscience 5, 799-802.

Joughin, I., Alley, R.B., 2011. Stability of the West Antarctic ice sheet in a warming world. Nature Geoscience 4, 506-513.

King, E.C., Hindmarsh, R.C.A., Stokes, C.R., 2009. Formation of mega-scale glacial lineations observed beneath a West Antarctic ice stream. Nature Geoscience 2, 585-588.

Kleman, J., Borgström, I., 1996. Reconstruction of Palaeo-ice sheets - the use of geomorphological data. Earth Surface Processes and Landforms 21, 893-909.

Kleman, J., Hättestrand, C., Borgström, I., Stroeven, A.P., 1997. Fennoscandian palaeoglaciology reconstructed using a glacial geological inversion model. Journal of Glaciology 43, 283-299.

Kleman, J., Hättestrand, C., Stroeven, A.P., Jannson, K.N., De Angelis, H., Borgström, I., 2006. Reconstruction of palaeo-ice sheets - inversion of their glacial geomorphological record., in: Knight, P.G. (Ed.), Glacier Science and Environmental Change. Blackwell Science Ltd, pp. 192-198.

Kleman, J., Applegate, P.J., 2014. Durations and propagation patterns of ice sheet instability events. Quaternary Science Reviews 92, 32-39.

Krabbendam, M., Eyles, N., Putkinen, N., Bradwell, T., Arbelaez-Moreno, L., 2015. Streamlined hard beds formed by palaeo-ice streams: A review. Sedimentary Geology 338, 24-50.

Laberg, J.S., Andreassen, K., Vorren, T.O., 2011. Late Cenozoic erosion of the high-latitude southwestern Barents Sea shelf revisited. Geological Society of America Bulletin 124, 77-88.

Lambeck, K., 1995. Constraints on the Late Weichselian ice sheet over the Barents Sea from observations of raised shorelines. Quaternary Science Reviews 14, 1-16.

Lambeck, K., 1996. Limits on the areal extent of the Barents Sea ice sheet in Late Weichselian time. Global and Planetary Change 12, 41-51.

Landvik, J., Bondevik, S., Elverhøi, A., Fjeldskaar, W., Mangerud, J., Salvigsen, O., Siegert, M., Svendsen, J.I., Vorren, T.O., 1998. The Last Glacial Maximum of Svalbard and the Barents Sea area: ice sheet extent and configuration. Quaternary Science Reviews 17, 43-75.

Larsen, N.K., Kjær, K.H., Funder, S., Möller, P., van der Meer, J.J.M., Schomacker, A., Linge, H., Darby, D.A., 2010. Late Quaternary glaciation history of northernmost Greenland – Evidence of shelf-based ice. Quaternary Science Reviews 29, 3399-3414.

NPD, 2015. Norwegian Petroleum Directorate FactMaps. NPD. Available online at : http://gis.npd.no/factmaps/html_20/ (accessed June 2015).

Nyland, B., Jensen, L. N., Skagen, J., Skarpnes, O. & Vorren, T. 1992: Tertiary Uplift and Erosion in the Barents Sea: Magnitude, Timing and Consequences. In Larsen, R. M., Brekke, H., Larsen, B. T. & Talleraas, E. (eds.): Structural and Tectonic Modelling and its Application to Petroleum Geology, 153-162. Elsevier, Amsterdam.

Ottesen, D., Dowdeswell, J.A., Rise, L., 2005. Submarine landforms and the recon- struction of fast-flowing ice streams within a large Quaternary ice sheet: the 2500-km-long Norwegian-Svalbard margin (57 degrees - 80 degrees N). Geological Society of America Bulletin 117, 1033-1050.

Ottesen, D., Stokes, C.R., Rise, L., Olsen, L., 2008. Ice-sheet dynamics and ice streaming along the coastal parts of northern Norway. Quaternary Science Reviews 27, 922-940.

Patton, H., Andreassen, K., Bjarnadóttir, L.R., Dowdeswell, J.A., Winsborrow, M., Noormets, R., Polyak, L., Auriac, A., Hubbard, A., 2015. Geophysical constraints on the dynamics and retreat of the Barents Sea ice sheet as a paleobenchmark for models of marine ice sheet deglaciation. Reviews of Geophysics 53, 1051-1098.

Patton, H., Hubbard, A., Andreassen, K., Winsborrow, M., Stroeven, A.P., 2016. The build-up, configuration, and dynamical sensitivity of the Eurasian ice-sheet complex to Late Weichselian climate and ocean forcing. Quaternary Science Reviews (in review).

Phillips, E., Everest, J., Diaz-Doce, D., 2010. Bedrock controls on subglacial landform distribution and geomorphological processes: Evidence from the Late Devensian Irish Sea Ice Stream. Sedimentary Geology 232, 98-118.

Pollard, D., DeConto, R.M., 2009. Modelling West Antarctic ice sheet growth and collapse through the past five million years. Nature 458, 329-332.

Polyak, L., Forman, S.L., Herlihy, F.A., Ivanov, G., Krinitsky, P., 1997. Late Weichselian deglacial history of the Svyataya (Saint) Anna Trough, northern Kara Sea, Arctic Russia. Marine Geology 143, 169-188.

Rasmussen, T.L., Thomsen, E., Ślubowska, M.A., Jessen, S., Solheim, A., Koç, N., 2007. Paleoceanographic evolution of the SW Svalbard margin (76°N) since 20,000 ^{14}C yr BP. Quaternary Research 67, 100-114.

Ritz, C., Edwards, T.L., Durand, G., Payne, A.J., Peyaud, V., Hindmarsh, R.C.A., 2015. Potential sea-level rise from Antarctic ice-sheet instability constrained by observations. Nature 528, 115-118.

Rüther, D.C., Mattingsdal, R., Andreassen, K., Forwick, M., Husum, K., 2011. Seismic architecture and sedimentology of a major grounding zone system deposited by the Bjørnøyrenna Ice Stream during Late Weichselian deglaciation. Quaternary Science Reviews 30, 2776-2792.

Rüther, D.C., Bjarnadóttir, L.R., Junttila, J., Husum, K., Rasmussen, T.L., Lucchi, R.G., Andreassen, K., 2012. Pattern and timing of the northwestern Barents Sea Ice Sheet deglaciation and indications of episodic Holocene deposition. Boreas 41, 494-512.

Rüther, D.C., Andreassen, K., Spagnolo, M., 2013. Aligned glaciotectonic rafts on the central Barents Sea seafloor revealing extensive glacitectonic erosion during the last deglaciation. Geophysical Research Letters 40, 6351-6355.

Salvigsen, O., 1981. Radiocarbon dated raised beaches in Kong Karls Land, Svalbard, and their consequences for the glacial history of the Barents Sea. Geografiska Annaler 63, 280-291.

Schoof, C., 2007. Ice sheet grounding line dynamics: Steady states, stability, and hysteresis. Journal of Geophysical Research 112, 1-19.

Siegert, M., Dowdeswell, J.A., 1996. Topographic control on the dynamics of the Svalbard-Barents Sea Ice Sheet. Global and Planetary Change 12, 27-39.

Siegert, M., Dowdeswell, J.A., Hald, M., Svendsen, J.I., 2001. Modelling the Eurasian Ice sheet through a full (Weichselian) glacial cycle. Global and Planetary Change 31, 367-385.

Siegert, M.J., Dowdeswell, J.A., 2002. Late Weichselian iceberg, meltwater and sediment production from the Eurasian High Arctic ice sheet: results from numerical ice-sheet modelling. Marine Geology 188, 109-127.

Sigmond, E.M.O., 1992. Berggrunnskart, Norge med havområder. Målestokk 1:3 millioner. Norges geologiske undersøkelse.

Solheim, A., Kristoffersen, Y., 1984. Physical environment Western Barents Sea, 1: 1,500,000; sediments above the upper regional unconformity: thickness, seismic stratigraphy and outline of the glacial history. Norsk Polarinstitutt Skrifter 179B, 3-26.

Solheim, A., Andersen, E.S., Elverhøi, A., Fiedler, A., 1996. Late Cenozoic depositional history of the western Svalbard continental shelf, controlled by subsidence and climate. Global and Planetary Change 12, 135-148.

Spagnolo, M., Clark, C.D., Ely, J.C., Stokes, C.R., Anderson, J.B., Andreassen, K., Graham, A.G.C., King, E.C., 2014. Size, shape and spatial arrangement of mega-scale glacial lineations from a large and diverse dataset. Earth Surface Processes and Landforms 39, 1432-1448.

Spagnolo, M., Phillips, E., Piotrowski, J.A., Rea, B.R., Clark, C.D., Stokes, C.R., Carr, S.J., Ely, J.C., Ribolini, A., Wysota, W., Szuman, I., 2016. Ice stream motion facilitated by a shallow-deforming and accreting bed. Nature Communications 7, 1-11.

Stokes, C.R., Clark, C.D., 1999. Geomorphological criteria for identifying Pleistocene ice streams. Annals of Glaciology 28, 67-74.

Stokes, C.R., Clark, C.D., Storrar, R., 2009. Major changes in ice stream dynamics during deglaciation of the north-western margin of the Laurentide Ice Sheet. Quaternary Science Reviews 28, 721-738.

Stokes, C.R., Spagnolo, M., Clark, C.D., Ó Cofaigh, C., Lian, O.B., Dunstone, R.B., 2013. Formation of mega-scale glacial lineations on the Dubawnt Lake Ice Stream bed: 1. size,

shape and spacing from a large remote sensing dataset. Quaternary Science Reviews 77, 190-209.

Stokes, C.R., Tarasov, L., Blomdin, R., Cronin, T.M., Fisher, T.G., Gyllencreutz, R., Hättestrand, C., Heyman, J., Hindmarsh, R.C.A., Hughes, A.L.C., Jakobsson, M., Kirchner, N., Livingstone, S.J., Margold, M., Murton, J.B., Noormets, R., Peltier, W.R., Peteet, D.M., Piper, D.J.W., Preusser, F., Renssen, H., Roberts, D.H., Roche, D.M., Saint-Ange, F., Stroeven, A.P., Teller, J.T., 2015. On the reconstruction of palaeo-ice sheets: Recent advances and future challenges. Quaternary Science Reviews 125, 15-49.

Stokes, C.R., Margold, M., Clark, C.D., Tarasov, L., 2016. Ice stream activity scaled to ice sheet volume during Laurentide Ice Sheet deglaciation. Nature 530, 322-326.

Svendsen, J.I., Gataullin, V., Mangerud, J., Polyak, L., 2004. The glacial history of the Barents and Kara Sea Region. Developments in Quaternary Sciences. Elsevier, pp. 369-378.

Syvitski, J., P. M. , Stein, A.B., Andrews, J.T., Milliman, J.D., 2001. Icebergs and the Sea Floor of the East Greenland (Kangerlussuaq) Continental Margin. Arctic, Antarctic, and Alpine Research 33, 52-61.

Sættem, J., Poole, D.A.R., Ellingsen, L., Sejrup, H.P., 1992. Glacial geology of outer Bjørnøyrenna, southwestern Barents Sea. Marine Geology 103, 15-51.

Thompson, T., 2004. Rose.NET. Available online at: http://mypage.iu.edu/~tthomps/programs/html/tntrose.htm (accessed January 2015).

Vorren, T.O., Laberg, J.S., 1997. Trough Mouth Fans - Palaeoclimate and ice-sheet monitors. Quaternary Science Reviews 16, 865-881.

Vorren, T.O., Landvik, J.Y., Andreassen, K., Laberg, J.S., 2011. Glacial History of the Barents Sea Region. In: Ehlers, J., Gibbard, P.L., Hughes, P.D. (eds.), Developments in Quaternary Science 15. Elsevier, Amsterdam, pp. 361-372.

Williams, J.D., 1980. Rosenet: a Fortran IV program for production of rose diagrams compatible with Gould or Calcomp plotting facilities. Computers & Geosciences 6, 95-103.

Winsborrow, M.C.M., Andreassen, K., Corner, G.D., Laberg, J.S., 2010a. Deglaciation of a marine-based ice sheet: Late Weichselian palaeo-ice dynamics and retreat in the southern Barents Sea reconstructed from onshore and offshore glacial geomorphology. Quaternary Science Reviews 29, 424-442.

Winsborrow, M.C.M., Clark, C.D., Stokes, C.R., 2010b. What controls the location of ice streams? Earth-Science Reviews 103, 45-59.

Winsborrow, M.C.M., Stokes, C.R., Andreassen, K., 2011. Ice-stream flow switching during deglaciation of the southwestern Barents Sea. Geological Society of America Bulletin 124, 275-290.